EVALUATING THE USE OF STRUCTURE-FROM-MOTION PHOTOGRAMMETRY IN THE EXCAVATION OF BURIED HUMAN REMAINS

by

Kathleen Flor-Stagnato, B.A.

A thesis submitted to the Graduate Council of
Texas State University in partial fulfillment
of the requirements for the degree of
Master of Arts
with a Major in Anthropology
August 2018

Committee Members:

Michelle Hamilton, Chair

Nicholas Herrmann

Daniel Wescott

Neffra Matthews

FAIR USE AND AUTHOR'S PERMISSION STATEMENT

Fair Use

Duplication Permission

DEDICATION

To Dad, Mom, Anne, Xavi, Felix, and Puss Puss, even if most of you can’t read this.

ACKNOWLEDGEMENTS

I would like to thank my adviser Dr. Michelle Hamilton for her guidance, support, and general awesomeness during the past two years. It has meant the world to me to be a part of this program; I can't imagine a better adviser, and I will always be grateful. I would also like to thank my committee members, Dr. Nicholas Herrmann, Dr. Daniel Wescott, and Neffra Matthews for guidance, support, and expertise. I would also like to acknowledge Dr. Daniel Wescott, Sophia Mavroudas, and all the donors who support our research at the Forensic Anthropology Center at Texas State. Without them, none of this would have been possible. Thank you to Dr. Kate Spradley, Dr. Todd Ahlman, and the rest of the anthropology department who have provided me with amazing opportunities and taught me how much I do not know. Thank you to my cohort and the friends I have made through this program, who volunteered to excavate my thesis with me, and donated so much of their time to help me succeed. To Susan Sincerbox and Autumn Lennartz, thank you for listening to my every complaint and always countering with encouragement, coffee, and comic relief. Caroline Znachko, I couldn't have made it through this year without your positivity and sisterhood. Special thanks to Briana New, Alexa Terry, Elaine Chu, and Audrey Schaefer for housing me when I was without, I couldn't have gotten here without you. Finally, thank you to my friends and family, who helped me stay grounded in life outside of Texas.

TABLE OF CONTENTS

Page

LIST OF TABLES

Table **Page**

LIST OF FIGURES

LIST OF ABBREVIATIONS

Abbreviation	Description
ASPRS	American Society for Photogrammetry and Remote Sensing
SfM	Structure from Motion
3D	Three dimensional
GIS	Geographic Information Systems
GPS	Global Positioning System
AAPA	American Association of Physical Anthropologists
AAFS	American Academy of Forensic Sciences
FACTS	Forensic Anthropology Center at Texas State
FARF	Forensic Anthropology Research Facility
DSEs	Disarticulated Skeletal Elements
CSB	Calibrated Scale Bar
GCPs	Ground Control Points
TS	Total Station
KPFS	Kathleen P. Flor-Stagnato, author
EYC	Elaine Y. Chu
CGS	Consistent Graduate Student
RGS	Random Graduate Student
BLM	Bureau of Land Management

JPEG ..... Joint Photographic Experts Group

PIX ..... Pixels

RMS ..... Root Mean Squared Error

GOL ..... Max Cranial Length from Glabella

I. INTRODUCTION

Photogrammetry is defined by the American Society for Photogrammetry and Remote Sensing (ASPRS) as "the science or art of obtaining reliable measurements from photographs" (Thompson et al. 1966:1). The field of photogrammetry has changed rapidly with the increasing ability for the public to access digital equipment necessary to complete photogrammetric projects (Walker and Alspaugh, 2013). Increasingly popular and accessible across many disciplines is the use of Structure from Motion (SfM) photogrammetry, which creates digital 3D models from photographs.

The use of this technology has not been well studied in forensic anthropological contexts. Baier and Rando (2016) evaluated the use of photogrammetry in a simulated mass grave and stated that accurate cranial and postcranial measurements would not be retrievable – post-excavation – from within the generated digital 3D model. However, other studies have explored the use of photogrammetry for archaeological site recording and have found post-excavation measurements within the SfM generated model not only possible, but accurate (De Reu, et al. 2014; De Reu, et al. 2013; Grussenmeyer and Perdrizet, 1996; Koenig, et al. 2017; Verhoeven 2011; Verhoeven, et al. 2012). The research presented here evaluates SfM photogrammetry in several ways. First, against other mapping and visualization methods such as hand-mapping and GIS. Specifically, it looks at time to collect photos and process models. Second, it evaluates the abilities of non-experts versus an expert in creating high quality models via several metrics. Third, this research compares traditional measurements of physical bones to measurements taken within the *in situ* digital models in order to understand the utility of SfM photogrammetry for use with human remains. Finally, this research will seek to develop a

workflow specifically for use in contexts containing human remains. In the following sections, I will discuss the history of photogrammetry and the development of digital photogrammetric workflows. Additionally, I will highlight important anthropological uses of photogrammetry. Finally, I will discuss the formal research objectives of this thesis.

History of Photogrammetry

Groundwork for the development for photogrammetry, like many other disciplines, began during the Italian Renaissance. Specifically, Leonardo da Vinci and his contemporary Albrecht Durer began to understand perspective, with Durer even inventing a machine to draw stereoscopic depictions (Walker and Alspaugh, 2013). During the 18th century, stereopair drawings utilizing those principles of perspective were used to produce topological maps. These developments in art and geodesy later allowed Poncelet to develop the tenets of projective geometry in the early 19th century, which provides most of the mathematical basis for photogrammetry (Walker and Alspaugh, 2013).

Photogrammetry can be divided into three time-periods which mainly correspond to the technology being used. The first is analog, which used film photography and manual point-matching workflows (Walker and Alspaugh, 2013). During the 19th century, both pinhole cameras and *camera lucida* were used to trace the projections of objects. However, until Daguerre invented the daguerreotype, there was no way to retain the image produced by the early imaging techniques. Soon after the daguerreotype was invented, film photography began. Immediately, people realized its potential to record topographic information and began to experiment with capturing aerial photographs. In

1858, Tournochon became the first aerial photographer when he captured photographs from a hot-air balloon over Bievre, France (Falkner, 1995). Figure 1 depicts a photo taken with the same technique in 1885 over Paris, France by Laussedat, another French photographer. (Thompson et al., 1996; Walker and Alspaugh, 2013). Figure 2 shows a drawing of the photo mount used by Laussedat to collect aerial images in hot-air balloons (Thompson et al., 1966). After developments in flight technology by the Wright brothers allowed for more control over the location of aerial photographs, Italians took the lead again, creating the first aerial map in 1913 (Falkner, 1995).

Figure 1. Photograph taken by Laussedat over Paris, 1885 (Laussedat, vol. 2, pt. 1, p. 83).

The potential for aerial photography and photogrammetry was immediately realized by various military powers. During the first World War, it was not used extensively due to a lack of standardization of equipment. However, the British,

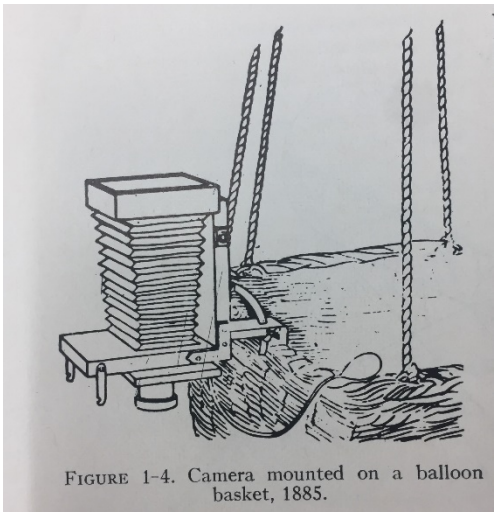

Figure 2. Camera rig on the side of a hot-air balloon basket (from Falker, 1995).

Americans, French, and Germans used handheld cameras held over the side of airplanes to gather intelligence (Falkner, 1995). In the interwar period there were many advancements which would later allow it to be used strategically as a remote intelligence gathering method. (Falkner, 1995; Walker and Alspaugh, 2013). During this time, photogrammetry becomes more widespread across industrialized nations. Between the two World Wars, the first aerial mapping companies had been started and color film was discovered. This lead to many more potential uses for aerial photography (Falkner, 1995).

During World War II, the Germans furthered technological advancements related to camera systems. The use by all combatants of infrared film, skilled photo-interpreters, and mass production helped fulfill the needs on both sides for detailed technical maps (Figure 3; Falkner, 1995). The developments during the Cold War were initially only used by the military, but soon found commercial outlets. The Cold War saw developments in aerial cameras, film, and remote sensors (Falkner, 1995).

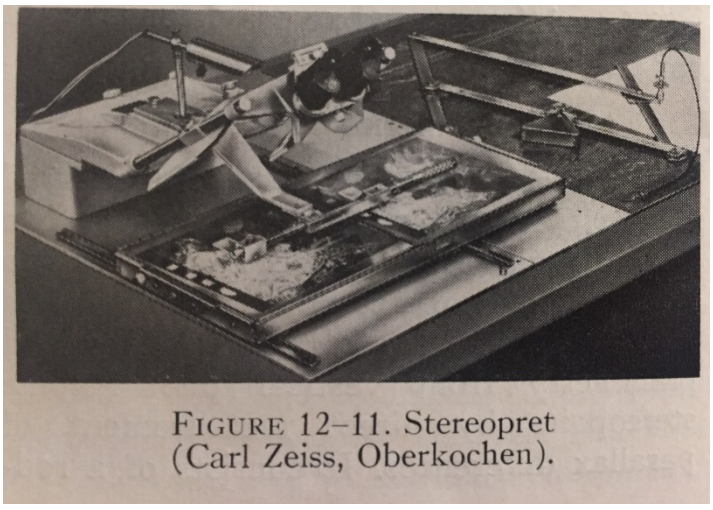

Figure 3. Analog stereoplotter, weighed 163 pounds (from Bodnar and DeAngelis, 1966).

With the introduction of computers, the analog era of photogrammetry ended, and the analytical era began (Walker and Alspaugh, 2013). This era was largely a transition between the manual, analog methods and the digital methods of today. Before the 1980s, photogrammetric data was drawn from aerial photographers through a detailed and complex workflow incorporating both technical expertise and artistic sensibilities (Falkner, 1995). The mapper used several tools to draw a map from the acquired aerial photographs (Figure 4). The photographs were analyzed as stereopairs, two images with significant overlap so that when aligned properly, a 3D image is created in the mind. Stereopairs use to concept of parallax to do this.

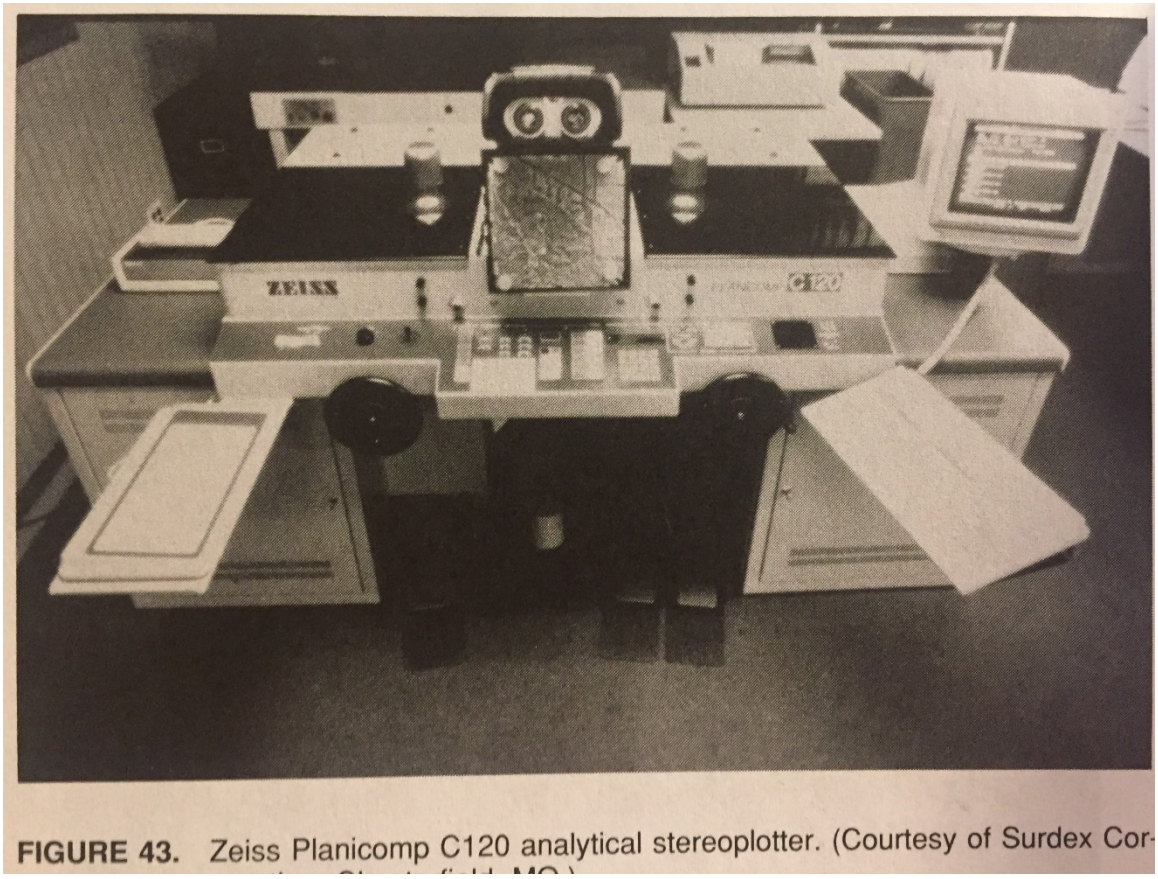

FIGURE 43. Zeiss Planicomp C120 analytical stereoplotter. (Courtesy of Surdex Cor-

Figure 4. Analytical stereoplotter (from Falkner, 1995).

Parallax is the property of optics that when an object of interest is viewed from two different vantage points, it appears to move. Imagine looking at your finger in front of your face. Close your left eye, and it is in one place. Close your right eye, and it appears to move. When the two views are combined, the brain synthesizes it into one location. Using this, points on photos could be tracked through space to create accurate maps and photogrammetric products. During this era, the production of map products from stereopairs often involved stereoplotters. These devices allowed the technician to view the stereopair of photos, and by orienting it to accurate spatial references and tracing the features on the stereopair, a map could be created (Falkner, 1995; Thompson et al., 1966; Walker and Alspaugh, 2013). Between the analog era and analytical era, stereoplotters utilized the same principles. It was the introduction of computers into stereoplotters which allowed for more detailed analyses (Falkner, 1995).

Computers made advances in analytical treatment of data recorded from photogrammetry much easier than it had previously been. Due to the quick pace of technological advancement, the analytical era quickly transitioned into the digital era of photogrammetry (example of equipment in Figure 5). Digital photogrammetry began with scanning of film photography, using various aerial films which had been in use for some time.

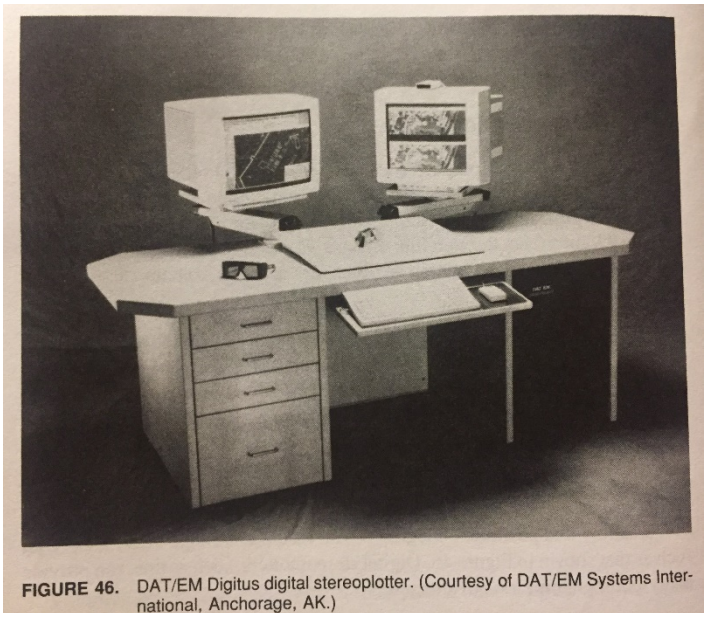

FIGURE 46. DAT/EM Digitus digital stereoplotter. (Courtesy of DAT/EM Systems International, Anchorage, AK.)

Figure 5. Digital stereoplotter (from Falkner, 1995)

Aerial film is typically large-format (10 in) wide, and the rolls of film ranged from 125 to 500 ft long (Falkner, 1995). Black and white film has three distinct layers: the base, the emulsion, and the antihalation backing. The base can be made of several materials, but it must not be flexible, especially for photogrammetry, to preserve the geometry of the captured image. The emulsion is what reacts to the light, and for color photos, lesser amounts of red-, blue-, and green-sensitive pigments are added to the emulsion. Most commonly used during this era were panchromatic (black and white) film, natural color film, infrared film, or color infrared film. During the 1980s, digital cameras became available to consumers, and the potential for photogrammetry grew (Walker and Alspaugh, 2013).

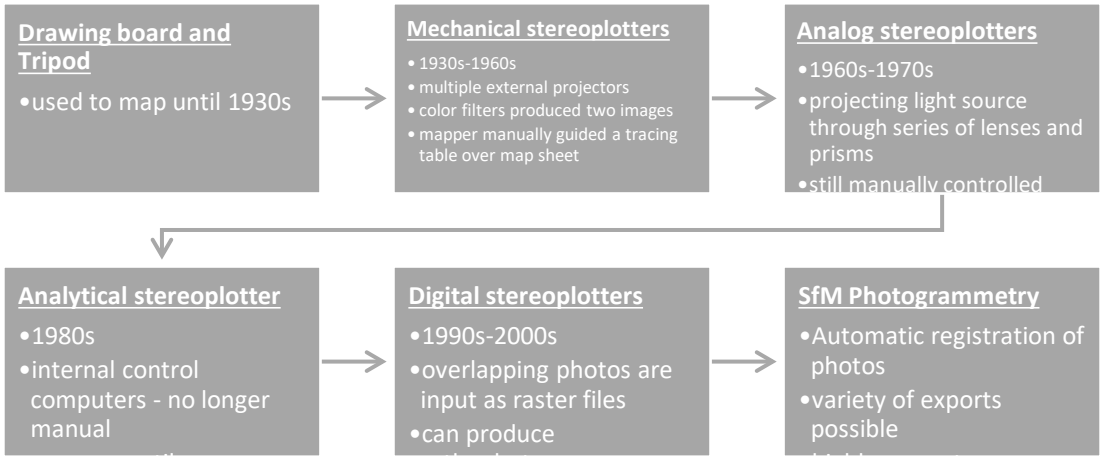

Figure 6. Progression of photogrammetric technology for mapping and interpretation. Timeline created by author from Falkner (1995), Thompson et al. (1966), and Walker and Asbaugh (2013).

Structure from Motion (SfM) photogrammetry was developed during the 1990s but has only become popular since about 2011, due to reduced cost and technical fixes which make it more useful and accessible to a general audience (Verhoeven et al., 2011).

SfM photogrammetry is most commonly accomplished using the computer program Photoscan by Agisoft (Agisoft Photoscan, 2017), although there are other freeware programs which have the same or similar capabilities (for a detailed list, refer to Granshaw, 2016). The algorithms used to match points in digital photographs are based upon the same principles developed during the analog era of photogrammetry. Points are detected and tracked between photographs and linked to form a 3D point cloud, from which a 3D mesh and other objects can be derived. These models can be georeferenced by inputting GPS locational data or scaled without GPS by using pre-calibrated scale bars of known dimensions which are highly accurate. Calibrated scale bars can increase the accuracy of the model, and georeferencing can aid in incorporating models with another GIS (Baier and Rando, 2016; De Reu, et al. 2014; De Reu, et al. 2013; Koenig et al. 2017; Verhoeven 2011; Verhoeven, et al. 2012).

Photogrammetry in Anthropology

Archaeological Applications of Photogrammetry

Digital photogrammetry has been in use within archaeology for over two decades. The earliest use is outlined in Doneus's 1996 presentation, "Photogrammetrical applications to aerial archaeology to the institute for prehistory of the University of Vienna, Austria." In this paper, Doneus outlined how archaeologists at the university used aerial photography combined with geophysical data and digital surface models to locate previously unknown archaeological sites. This early paper was essential in promoting the use of photogrammetry for archaeology. While they used aerial imagery, other archaeologists at the time were exploring close-range photogrammetry to document their sites. Grussenmeyer and Perdrizet were some of the first to explore this, and

integrated photogrammetry in their research to document a Roman forum in Sarmizegetusa, Romania (Grussenmeyer and Perdrizet, 1996). Their workflow is an example of the analytical era processes, as they used a small-format camera and film photography which was processed in the field for data collection. Processing and analysis of the data incorporated computers and stereoplotters. This early study concluded that the use of close-range photogrammetry was beneficial in terms of time for mapping and the accuracy of map products, especially on archaeological sites with complex features (Grussenmeyer and Perdrizet, 1996)

Koistinen et al. (2000) were some of the first archaeologists to integrate and plan photogrammetric data collection into their excavation plans. They also were early to acknowledge the ability for collected images and models to be revisited once the field season has ended. This is an advantage of using photogrammetry touted by many later archaeologists (De Reu et al., 2013; De Reu et al., 2014; Koenig et al., 2017; Verhoeven, 2011; Verhoeven, 2012). The transition to the digital era of photogrammetry was spearheaded in archaeology by Georgiadis, et al. (2000). This paper explored the use of digital cameras, and computer-based workflows for same-day processing of collected photogrammetric data and mapping of sites with complex stratigraphy and features. The main object created with the photogrammetric workflows on site was accurate orthophotos (rectified photos which eliminate distortions due to the camera lens and perspective), however, Georgiadis, et al. (2000) also explored building 3D models of artifacts recovered at their site. Overall, this paper was important in highlighting the usefulness in both the field and in lab of the photogrammetric data and hinted at how the technology would be used in the future.

Between 2000 and 2006, it is clear from the literature that there was a meaningful change in the accessibility of photogrammetry and an increase in its use at archaeological sites. Some researchers began to publish their findings on the use of photogrammetry to record artifacts (Kalantari and Kasser, 2006), the use of photogrammetry in underwater archaeology (Drap, et al. 2006), and documentation and preservation of cultural heritage (Bitelli, et al. 2006; Doneus, et al. 2006), while citing its low-cost and ability to be used by non-technical experts (Bitelli, et al. 2006; Boochs et al., 2006; Drap, et al. 2006; Doneus, et al. 2006; Kalatari and Kasser, 2006; Patias, et al., 2006).

Due to further technological developments, decreases in cost, and increasing accessibility of photogrammetry, its implementation in archaeology has continued to grow. Documentation of archaeological excavation relies heavily on photography, so much of the equipment necessary for photogrammetry is already present at a site.

Agisoft Photoscan, a computer software program which uses Structure from Motion algorithms to match photos and create photogrammetric models, was released in mid-2010 (Verhoeven, 2011), and was rapidly integrated into archeological research. Researchers including Verhoeven (2011), Verhoeven et al. (2012), and De Reu (2013) were some of the first in archaeology to validate and implement this fully digital methodology into archaeological workflows and site excavation. Their research was focused on evaluating how easy it was to integrate into the excavation process, and its potential to integrate historic imagery and explore heritage management concerns. They were successful in their endeavors and paved the way for many further studies to incorporate this technology (e.g., Douglass et al., 2011; Howland et al., 2014; McCarthy, 2014; Sanger, 2015). Other studies have focused on using SfM photogrammetry to

document artifacts in the lab and to perform analyses. These have documented the flexibility of SfM for both documentation and analysis. Porter et al. (2016) used SfM photogrammetry to document lithic artifacts, Koutsoudis et al. (2013) evaluated close range SfM photogrammetry on a low-relief object against laser scanning, Gonzalez et al. (2015) used what they termed "microphotogrammetry" to characterize cut marks on bone, and finally, Evin et al. (2016) used photogrammetric models and geometric morphometrics of wolf crania to study dog domestication. These various uses were just the tip of the iceberg for photogrammetry. It is a cost-effective and easily integrated method/technology, and can provide diverse types of data, along with helping to record sites or artifacts before destructive analysis. As an inherently destructive process, archaeological investigations should incorporate all available methods to digitally document and preserve this cultural heritage.

Photogrammetry in Biological Anthropology

Unlike archaeologists, biological anthropologists have not widely explored the use of SfM photogrammetry. Baier and Rando (2016) remains one of the few published papers citing its use with human remains. There have increasingly been more poster presentations on its use at both the AAPA and AAFS conferences, but little research has been published. Furthermore, many of these studies use plastic replicas of human bone, as Baier and Rando (2016) did. While the replicas may be accurate in terms of features, length, and dimensions, if made of plastic they are often far shinier than human skeletal materials, and this reflectivity can cause issues in the creation of accurate 3D models. Furthermore, actual human osteological elements should be used in SfM research to generate more accurate and realistic results, since as a remote-sensing technology,

photogrammetry is completely safe, non-destructive, and non-damaging to human remains.

Photogrammetry has many potential benefits for biological anthropology in addition to forensic anthropological contexts. Historic and prehistoric skeletal remains often have issues of preservation, since over time and depending on soil chemistry, human bone can deteriorate, leading to damage upon removal from the burial matrix. Excavation of fossilized hominid remains are also a concern to paleoanthropologists. These are examples of specific niches which SfM has the potential to fill. If, through my research, it is shown that accurate skeletal measurements can be taken from *in situ* human remains, it would allow for study on bones too fragile to be exhumed from their context, or for remains which may fracture upon removal.

Mapping complex forensic mass graves with SfM photogrammetry has the potential to improve current methodology due to its low cost, speed, and more complete representation of a 3D scene. While mapping with a total station provides accurate measurements and data analysis potential, SfM photogrammetry offers a way for researchers to represent and re-analyze the scene. Traditional archaeological techniques rely upon a squared grid to maintain provenience, but Willis et al. (2016) have explored the use of a non-unit-based approach and found it beneficial and easy with SfM documentation. Human remains, particularly in commingled mass graves, do not conform to 1 m x 1 m units or neat 10 cm levels (Tuller and Đurić' 2006). SfM allows for this complexity to be accurately recorded, represented, and reexamined.

Rationale for SfM Photogrammetry use in Mass Grave Excavations

Crises in human rights violations increased the necessity for forensic anthropological and archaeological expertise in conflict and mass grave excavation scenarios (Haglund 2001; Schmitt 2001; Simmons 2001). Technological advances beyond traditional hand mapping spurred the use of total stations to map elements on *x, y,* and *z* planes, which allowed for more flexibility than traditional excavation grid and tape measure mapping (Tuller 2012; Tuller and Hofmeister 2014), although total stations require special expertise in operating and processing the data. The introduction of SfM offers a potential alternative to technologies like total stations and GIS which are expensive and difficult to learn because SfM is a faster, more accessible way to collect spatial data (Baier and Rando 2016; De Reu, et al. 2013; Verhoeven, et al. 2012). Rather than painstaking data collection of many hundreds of points with a total station, along with separate rounds of photographs, 3D spatial data can be created from photographs and processed into a SfM model, streamlining the entire data collection process. Another consideration for SfM use in mass burials is the potential lowered costs of excavation, the lowered time requirements, and the possibility of post-excavation reassociation of remains. Depending on your licensing and the desired capabilities of the software, a digital camera capable of taking usable photos and an Agisoft Photoscan license can cost from $800.00 to $4500.00. A total station costs at least $4500.00 for the machine alone, not including accessories like tripods, data collectors, and prisms.

Terrestrial laser scanners are even more expensive, costing at least $20,000.00 for hardware alone. Structure from Motion photogrammetry can produce models which rival those of other technologies as a much lower cost.

Research Questions

Given the information reviewed in this section, the research questions of this thesis are as follows:

1. Does SfM photogrammetry provide measurable advantages over other current documentation methodologies used in forensic anthropological contexts?
    a. *Time required to document the scene; e.g., hand-mapping versus total station versus photogrammetry*
    b. *Ease of use for producing accurate/usable models (defined as a model which meets minimum error specifications)*
2. Can accurate cranial and postcranial measurements be retrieved from within the SfM-generated 3D model?
3. If SfM photogrammetry provides advantages over other methods, and if accurate osteometric measurements can be retrieved from within the photogrammetric model, can an SfM-focused standard forensic archaeological set of best practices be developed?

Impact of this Research

The use of SfM photogrammetry has not been well studied in forensic anthropological contexts. Baier and Rando (2016) evaluated the use of SfM in a simulated mass grave and stated that accurate cranial and postcranial measurements were not retrievable - post-excavation - from within the SfM-generated 3D model. However, other studies have explored the use of SfM for archaeological site recording (i.e., not mass graves) and have found post-excavation measurements within the SfM-generated 3D model were not only possible, but accurate (De Reu, et al. 2014; De Reu, et al. 2013;

Koenig, et al. 2017; Verhoeven 2011; Verhoeven, et al. 2012). The contradict ion in findings from Baier and Rando's mass graves study needs to be examined considering the multitude of archaeological studies that have found accuracy in measurements possible using SfM.

If SfM photogrammetry can be used to accurately capture measurement and spatial data from mass graves, the development of a standardized protocol for SfM use in forensic burial contexts is possible. My research project will test whether an SfM-generated 3D model of a mass grave containing multiple skeletonized and decomposing human remains can be used to accurately assess *in situ* osteological measurements as well as spatial relationships of the bodies within the burial for use in the development of such a protocol.

Assessment of the validity of SfM as a documentation method for *in situ* human remains has relevance for a number of applications, including paleoanthropological, bioarchaeological and forensic contexts. If this project shows that SfM can accurately capture measurement and spatial data from complex burial contexts, developing an SfM standardized protocol for human burials is warranted. For mass graves, SfM offers a fast, inexpensive, and easy to learn method of documenting a crime scene. For human rights investigations, which operate on tight budgets and timelines, an SfM burial protocol could streamline best practices. This technology also has the potential to allow continued study on human remains which are fragile or inaccessible to researchers. Understanding the strengths and weaknesses of SfM in relation to human remains can help assess if it should be more commonly used over or in tandem with other documentation methods. Furthermore, by definition, the purpose of photogrammetry is to obtain measurements. If

this technology cannot be used to obtain those, then it cannot rightly be called photogrammetry. The impact of this technology centers on its ability to provide metric and spatial data combined with accurate imagery.

II. MATERIALS AND METHODS

Sample Selection

For this research, five sets of human remains and 22 assorted disarticulated human skeletal elements from the Forensic Anthropology Center at Texas State's (FACTS) Willed Body Donation Program were buried to simulate a mass grave. Donor bodies were chosen from those who had completed their roles in the Forensic Anthropology Research Facility's (FARF) ongoing longitudinal study.

Four of these donor bodies were fully articulated and partially skeletonized at the time of burial (D41-2016, D46-2016, D58-2016, and D59-2016). These four donors were selected for placement within the grave based upon their morphological and demographic differences to ensure pair-matching would be possible in the case of commingling. A fifth set of remains (D61-2016) was buried in the grave as well, though during their time in the longitudinal study they had been heavily scavenged by both ants and small rodents, leading to almost complete disarticulation and skeletonization before burial. Partially skeletonized remains were chosen for this study to minimize the amount of time needed to reach complete skeletonization while buried. Select demographic data for all donors buried in this study is presented in Table 1.

Additionally, 22 assorted human disarticulated skeletal elements (DSEs) were obtained from other donor bodies who had already completed the decomposition process. These skeletonized elements were used to further simulate a commingled mass grave, and to ensure that in the case that the complete donor bodies did not decompose completely, single skeletal elements would still be present to measure within the *in situ* 3D model. Demographic data for the DSEs are included in Table 2.

Table 1. Demographic data for selected complete donors who were buried.

Demographic data on complete donors placed in grave			
Donation Number	*Sex*	*Age*	*Living Stature*
D41-2016	F	77	142
D46-2016	F	47	173
D58-2016	M	63	187
D59-2016	M	69	177
D61-2016	F	74	163

Table 2. Demographic data for additional donors whose disarticulated skeletal elements were buried.

Demographic data for buried DSEs					
Donation Number	*Elements used*	*Tag number*	*Sex*	*Age*	*Living Stature*
D44-2012	Atlas	16	M	79	184
	Axis	17			
D19-2014	L clavicle	5	F	77	157.5
	Mandible	6			
	R scapula	7			
	R radius	8			
D46-2014	L ulna	21	F	81	163
	Cranium	22			
D01-2015	R clavicle	15	M	59	179
D07-2015	Sacrum	1	M	53	183.5
	R os coxae	2			
	R humerus	3			
	L5	4			
D09-2015	L femur	13	F	74	158
	L fibula	14			
D36-2015	L scapula	9	M	57	176
	R tibia	10			
	R fibula	11			
	Cranium	12			
D15-2016	L os coxae	18	F	53	166.5
	L tibia	19			
	Thoracic vertebra	20			

Preparation and Placement

A large grave was excavated by backhoe and shovel to the size of 3 m x 2 m x 50 cm to accommodate all research subjects and to mimic a mass/clandestine burial. The depth of the grave was limited by both large subsurface boulders and clay-heavy subsoils. This research was completed at the Forensic Anthropology Research Facility, which is the outdoor research facility associated with the Forensic Anthropology Center at Texas State University in San Marcos, Texas.

In preparation for placement, a skeletal inventory was taken for the five complete donor bodies, during which hands, feet, and any other loose skeletal elements were removed from the body to prevent commingling of these smaller bones within the grave.

D61-2016 had undergone intensive scavenging during caged decomposition. Additionally, this donation was placed in a "double cage" with D62-2016, which remained in the double cage after the skeletal inventory was conducted on D61-2016. Because of these factors, the skeletal inventory completed on D61-2016 was done incorrectly and resulted in two sets of right ulnae and radii being placed within the grave. The correct elements were reassociated after excavation and disarticulation of D62-2016.

The disarticulated skeletal elements (DSEs) were labeled with numbered metal tags and assigned a number 1-22 to maintain association and inventory control. Labeling the DSEs was essential for later reassociations.

Placement of the five bodies and 22 DSEs within the empty grave occurred on July 1, 2017. A team of graduate students first transported the inventoried complete remains to the area of the grave using backboards. Donors were placed into the grave individually. After each donor was placed into the grave, a round of photos was taken to

document the original position of the remains. Photo logs (Appendix A) were used to detail the parameters of the photos taken. Additionally, once all complete donors and all 22 DSEs had been placed, another round of photos was completed as a representation of overall positions before burial. Seven ground control points were included within the grave and recorded using a Sokkia SET530R total data station. Positions of the five complete donors and seven ground control points are shown in Figures 7 and 8. The grave was then backfilled.

Excavation and Documentation

Excavation of the grave began approximately three months later, on September 22, 2017. The grave had become somewhat overgrown, and it was necessary to cut back the vegetation with a weed wacker. After vegetation was cleared, photo positions were laid out for the dome model (see "Dome Model" section later in this chapter). Overall, 60 photo positions were laid out in a rounded rectangle around the grave. For the long edges, there was a 10-degree difference between photo positions. On the corners, the angle changed by only 5-degrees to ensure proper overlap for the photos. Photo positions were calculated using a Suunto sighting compass. Once these had been established, nails were placed in the ground and spray painted to ensure visibility. No photo positions were laid out for the plane model (see "Plane Model" section later in this chapter) because some would have been inside the grave, which would have lead to inconsistent results between levels. Additionally, it is easier to ensure 60 percent overlap of plane photos in the viewfinder of the camera than it is to ensure a 10-degree change between photos of the dome model.

After the photo positions were laid out, the four calibrated scale bars were nailed into position around the grave. CSB 023 was later removed as it had been displaced during excavation and could no longer ensure accuracy. A 3 m x 2 m grid was laid out which encompassed the entire grave. All six units were hand-mapped in plan by graduate students who had experience in archaeological recording techniques for the surface level and bottom of level 1. For level 2, once all skeletal material was visible, only two units were mapped. These were unit 0N 1E and 1N 1E. These hand drawn maps were then compared to maps drawn from the orthomosaics produced from the digital models. Orthomosaics are rectified photographs generated within the software by correcting the photographs used to produce the SfM model for perspective distortion and stitching them together to provide a single rectified model photo mosaic. The grave was excavated in 20 cm levels to ensure some vertical control while enabling rapid recovery of the buried remains. All human remains present within the grave were completely exposed by September 24, 2017, however additional excavation was needed to remove remains from the grave. Final excavations were completed on October 15, 2017.

Photogrammetry

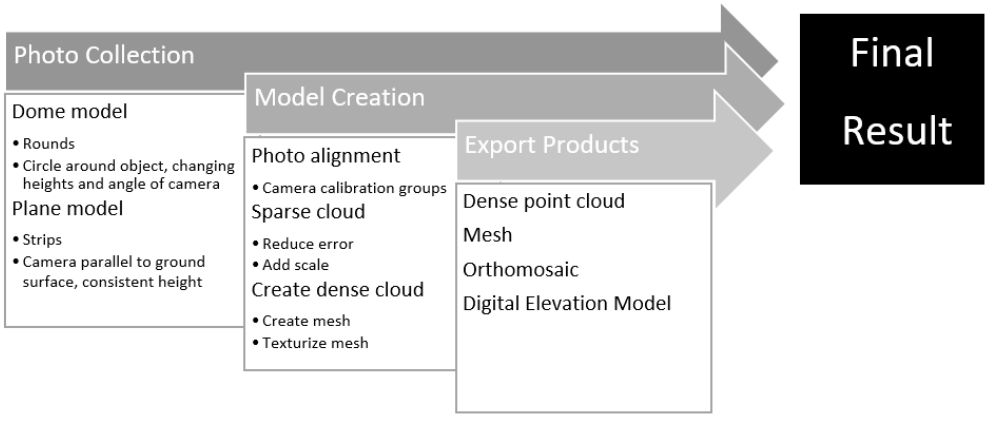

Figure 7. Chart of overall process and potential outputs of photogrammetric process. Image created by author.

Figure 8. Orthomosaic showing locations of complete donors and DSEs at placement. Grid north is up.

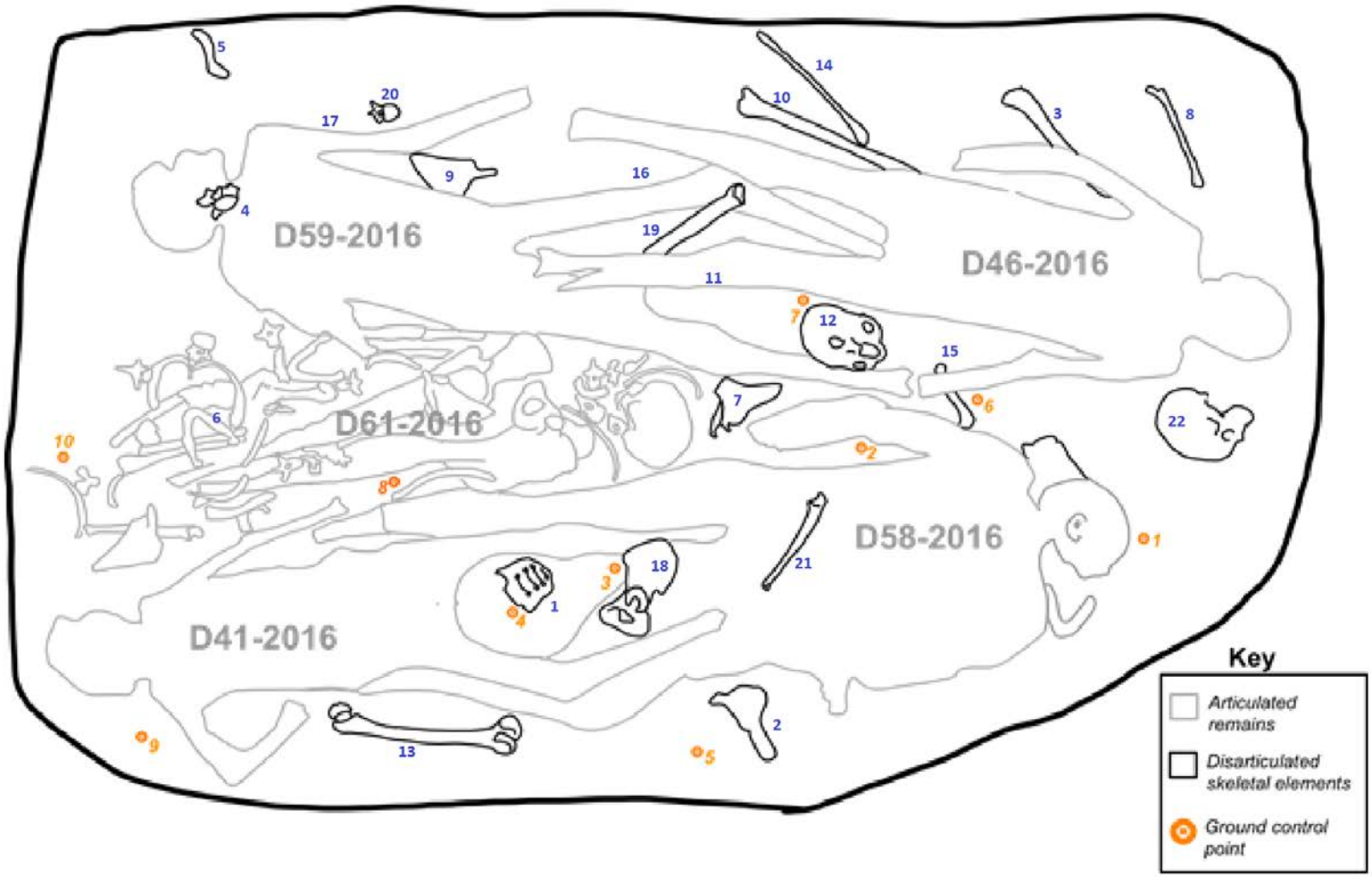

Figure 9. Digitally generated schematic showing locations of complete donors and DSEs at placement. Grid north is up. Produced by author by tracing orthomosaic.

Image Collection

Photographs were taken using an Olympus OM-D E-M5 Mark II 16-megapixel camera. This camera was attached to a monopod which was adjustable for height between 3 and 6 feet. Additionally, a remote shutter was used to make photography at difficult angles easier. For each set of photos taken, two separate image collection strategies were used. These are outlined in (Matthews, 2008), and when joined together in Agisoft Photoscan allow for better camera calibration, which increases the accuracy of the geometry of points and final product. All photos were taken on manual mode, with aperture fixed at 5.6 and ISO fixed at 200. Shutter speed was variable, though all photos for each strip/round were kept at the same specifications to improve camera calibration. Focal length was also kept the same at 14 mm and as close to a universal focus as possible. Additionally, photos were saved in the camera in both the RAW file format and JPEG, to preserve as much information as possible and ensure the ability to edit the photos later. Following these standardized practices allows for accurate camera calibration – changes between each photo changes the focal length and will result in a non-standard distance between lens and object resulting in bad geometry.

Plane Project

The first set of photos completed at each excavation level was a “plane” project. For the project, the camera is kept parallel (nadir) to the ground surface. Photos are taken in “strips” where each photo must overlap approximately 60 percent with the consecutive photos, and each strip should overlap with the previous strip by 20 percent. The overlap between consecutive photos is termed endlap, and the overlap between strips is termed

sidelap. At least three strips need to be completed, but enough should be completed that it covers the entire area plus buffer which is desired in the final product.

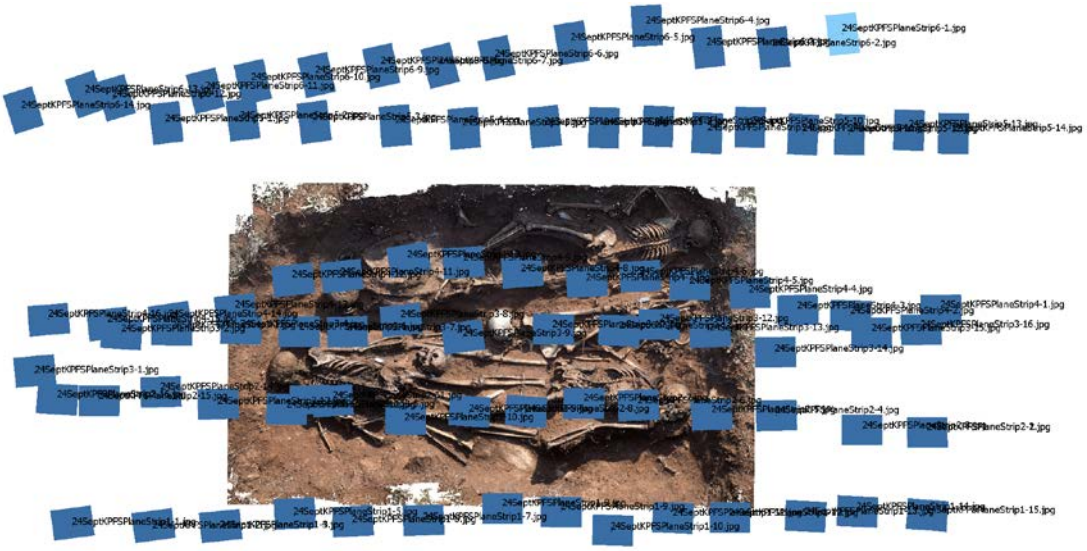

Figure 10. Screenshot of Level 2 plane model from nadir position with camera positions in blue.

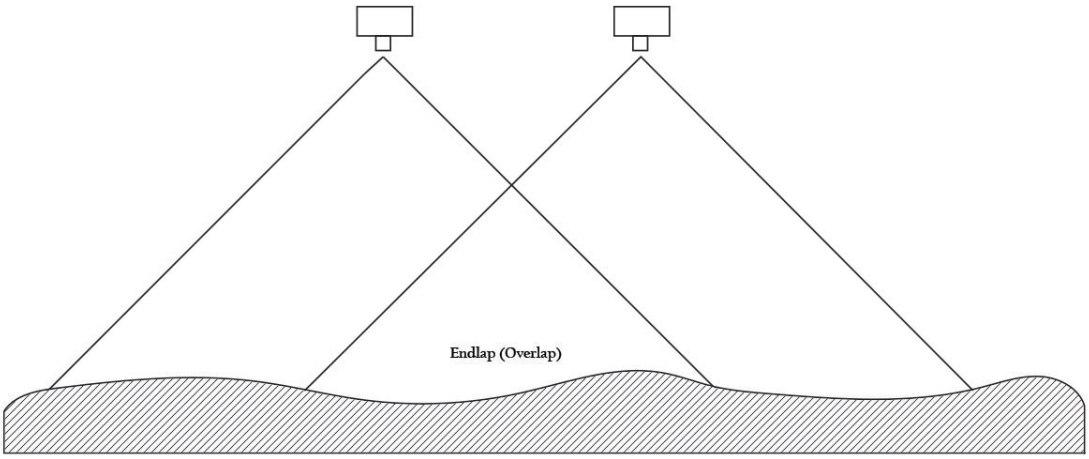

Figure 11. Diagram of ideal photo overlap for plane model - viewed from side showing two consecutive photos. Endlap should be 60 percent. These two cameras would be a stereopair. Image created by author.

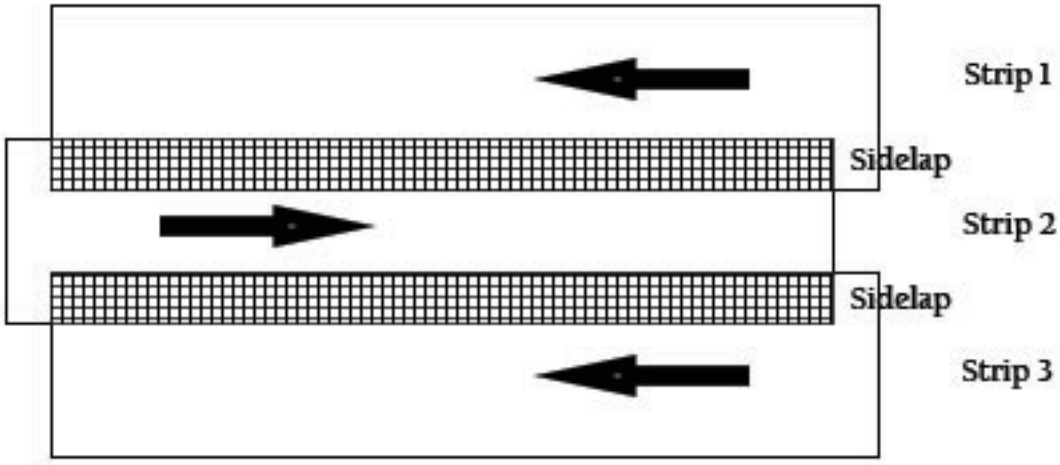

Figure 12. Showing overlap between consecutive strips in a plane model. Ideal sidelap is 20 percent. Arrows indicate the direction of travel, grid pattern indicates the areas of 20 percent sidelap.Image created by author.

The first strip can have the camera oriented in any direction, but the second strip requires the camera to be at 90 degrees, and the third would require a rotation of 270 degrees. The plane model is often the most spatially accurate model but can have gaps due to the lack of perspective views on the object. For this reason, it is important to integrate another photo collection strategy.

Dome Project

The second set of photos which was completed is a “dome” project. For this project, several rounds of photos are completed, where one round means one complete circle around the object of interest at a constant height. Due to the dimensions of the grave, there were 61 photos in a complete round. Four rounds were completed for each dome model, with a difference of one foot in height between each round. This photographic strategy allows for multiple views of the same object, ensuring that there were not gaps when the models were processed.

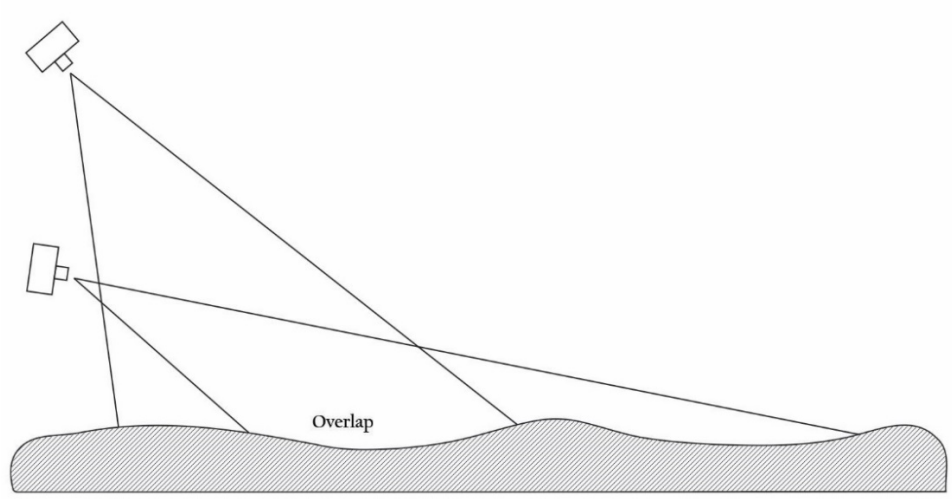

Figure 13. Simplified photo collection strategy for dome model with high oblique photo and low oblique photo. Image created by author.

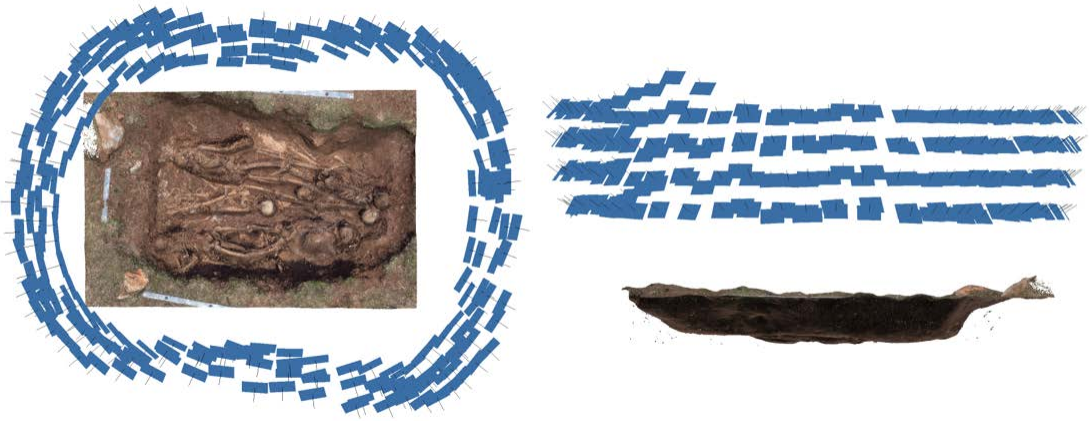

Figure 14. Level 2 Dome model photo positions from above (left) and side (right).

In cases where close-up photos were determined to be necessary to capture adequate detail, a set of photos was taken at half the distance from the normal photo positions and the close-up location. This ensured that points within the detail photo would be trackable by the software during processing.

To test timing and ease of taking photographs, the photos for the plane and dome model were collected by 1) the author (KPFS), 2) one consistent student (EYC), and 3)

random graduate students who had not done photogrammetry previously (multiple students, designated as “RGS” for random graduate students). Photos were collected by each student and the author at the surface, the bottom of each 20 cm level, and upon complete exposure of all remains. The photos were recorded on data sheets provided in Appendix A. Ease of learning was quantified via evaluation of time to complete both a dome and plane project and the quality of the model generated from each set (See “Statistical Analysis” section in this chapter for details on assessment of model quality). The author serves as an expert, whereas the consistent student helps us understand the learning curve, and the random untrained students act as beginners for a test of initial difficulty of learning.

Spatial Control

At the time of donor placements within the grave, seven ground control points were also placed and recorded with a total data station (TDS). These were used to scale the model and tie it to real world coordinates. Additionally, calibrated scale bars (CSBs) specifically designed for photogrammetry by the Bureau of Land Management (BLM) were included in the photos. The CSBs allow for submillimeter accuracy within the 3D model but cannot tie the model to real world geographic coordinates.

Processing

RAW images were edited using Adobe Lightroom software to standardize exposure, contrast, and apply vignette. Once edited, they were exported as JPEG with minimal compression. Each strip or round was separated into its own camera calibration group in Photoscan. This aids in photo alignment and accuracy in cases where any of the

specifications (like focal distance, shutter speed, etc.) may affect the distance between the camera lens and the object of interest, which affects the geometry of the points.

Both the plane and dome model photographs were loaded into the same Photoscan project and processed in a single chunk. After separation into camera calibration groups based on strip or round, they were aligned on high with 60,000 key points limit and no generic preselection. Disabling generic preselection allows for more points to be aligned, as it does not limit the photos it searches through for matching points. All processing occurred on an ASUS ZenBook Pro UX501VW. This laptop has an Intel Core i7 Processor, with 16GB RAM, NVIDIA GeForce GTX 960M graphics card, along with 1tb hard drive and 256 solid state drive.

After initial alignment, a sparse point cloud was created. A sparse point cloud consists of the points matched between the photos in the model. By using the gradual selection tool, it is possible to select and remove points with high error or bad geometry. All specifications used during model processing are presented in Table 3, and data sheets used to record model parameters are included in Appendix B. Once these parameters had been reached, calibrated scale bars (CSBs) and/or ground control points were used to scale the model. Once this was done, the bounding box was edited to eliminate unnecessary processing, and the dense point cloud was created.

Skeletal Measurements

Skeletal measurements were performed on the digital, *in situ* models of the grave using Photoscan's built-in measure tool. While four of the five complete donors were skeletonized upon excavation, D59-2016 was excluded from the measurement process as this individual was still mostly fleshed upon excavation. For each individual, all possible

measurements were taken following Howell's procedures (Howells, 1973) for cranial measurements and Zobeck's (1983) for postcranial measurements. Digital measurements of the disarticulated skeletal elements from the *in-situ* model were also completed for all elements which were possible. Sets of digital measurements were repeated on all elements a total of three times in order to assess the repeatability of accurate measurements. Physical measurements of the bones were completed after excavation and laboratory processing and cleaning of the remains using the standard metric procedures outlined in Howell's and Zobeck's. These measurements were also repeated three times to validate intraobserver error.

Table 3. Summary of the parameters used during model processing in Agisoft Photoscan.

Summary of Parameters for Processing in Agisoft Photoscan			
	Quality Processed	*Parameters*	*Desired Parameter Value*
Photo Alignment	High	Key point limit	60000
		Tie point limit	0
		Generic preselection	Disabled
Gradual Selection		Reconstruction uncertainty	10 (plane), 15 (dome), or no more than half of the points selected
		Projection accuracy	2 or no more than half of the points selected
		Reprojection error	0.3 or no more than 10 percent points selected
Dense Point Cloud	Medium		

Statistical Analysis

Digital measurements were compared to physical measurements using a Wilcoxon signed rank test performed using RStudio (RStudio Team, 2015). This statistical test is a non-parametric test related to the t-test which compares the means of two samples. Sample one was the three repeated digital measurements, and sample two was the three repeated physical measurements. It was used due to the small sample size (n = 3 measurements) which did not meet the assumptions of parametric tests. This test has a null hypothesis that the two samples are from the same population. If this null hypothesis is rejected, it can be concluded that the two samples are not from the same population. Due to many ties in the data, exact p-values were not able to be calculated in r, however this did not affect the results of the analysis.

Model quality and the ease of learning photogrammetric techniques was assessed quantitatively and qualitatively. For the photo collection stage, total time to collect all photos was calculated. After processing, models with photographs taken by the author, the consistent student, and the random students were compared based on the root mean square error. Additionally, the number of photos which successfully aligned on the first attempt in Photoscan was also compared. The final quantitative measure was how close the models got to the ideal processing parameters outlined in Table 3. Qualitative comparison was based on number of holes in the generated mesh, and how high the resolution of the output model was.

III. RESULTS

Photogrammetry Ease of Use and Learning Tests

Photo Collection

Photo collection time varied, with an average time for all photographers (KPFS, EYC, and RGS) being 48 minutes, and the median being 40 minutes to collect all photos for both plane and dome models.

The photo times for the author (KPFS) decreased with each set collected. The set for the surface model took 50 minutes, level 1 took 40, while the final level 2 model took 37 minutes.

The consistent graduate student (EYC) decreased her time from 60 minutes for the surface model, to 41 minutes for level 1, and 32 minutes for the level 2 model. While EYC's photographs were collected more quickly than the author's in some cases, her RMS reprojection error remained higher in all three models.

Photo collection times for the random graduate students (RGS) varied between 37 and 100 minutes to collect the necessary photos. However, two-thirds of the random graduate students collected their photos in 40 minutes or less. Their RMS reprojection error were comparable to both the author's and the consistent graduate student's.

Quality of 3D Models Produced

All processing in Agisoft Photoscan was completed by the author and followed standard error reduction processes. All photographers (author, consistent graduate student, or random graduate students) produced models where 99 percent of the photos aligned. Additionally, the models produced for each level were consistent between photographers for how many of the error reduction parameters could be reached. None of

the models processed by any photographer could reach the recommended level of 10 for reconstruction uncertainty, however 77 percent of the models (7 out of 9) were able to reach a reconstruction uncertainty level of 16. Reconstruction uncertainty is a measure of how accurate the positioning of points in space is, and while 10 was the desired level, 16 is within acceptable ranges (Matthews, personal communication). Level 2 models were unable to reach the projection accuracy of 2 which was the goal, but they were able to reach a projection accuracy of 3. This is another measure of how accurate the positing of points in space is. For all nine models, reprojection error was able to be brought to 0.3, which is the recommended level. Reprojection error is the accuracy of point positioning and is measured in pixels. The level of 0.3 mean that there would be a 0.3 pixels reprojection error for each point.

All processing occurred on an ASUS ZenBook Pro UX501VW. This laptop has an Intel Core i7 Processor, with 16GB RAM, NVIDIA GeForce GTX 960M graphics card, along with 1tb hard drive and 256 solid state drive. Processing time for both photo alignment and dense cloud creation varied between photographers and models, due to varying numbers of photos. The average computer processing time to align photos and create a sparse cloud, with generic preselection unselected, key point limit of 60,000, and no tie point limit was 14 hours. Average time to construct a dense cloud with quality set at medium was 16 hours. Together, this means that on average it took approximately 30 hours of processing time in Agisoft to create a model using these specifications

The average ground resolution achieved within the models was .51 mm/pixel, which means that for each pixel in the model, it represents .51 mm on the ground.

Table 4. Summary of model properties and quality (KPFS = author, EYC = consistent student, and RGS = random graduate students). See Appendices D, E, F for models.

Surface Model Summary of Results											
	Photo collection time (mins)	*Total No. Photos*	*Photo Alignment Percentage*	*Tie points*	*Time to Align Photos*	*Parameters Reached - Percent*	*Time to Dense Cloud*	*Ground Resolution*	*RMS reprojection error*	*Max reprojection error*	*No. points - Dense Cloud*
KPFS	50	436	100	392855	14 hours	66	26 hours	0.479 mm/pix	0.128437 (0.26165 pix)	0.320362 (1.1606 pix)	3.9 million
EYC	60	408	100	391669	11.75 hours	66	15 hours	0.466 mm/pix	0.128137 (0.262072 pix)	0.31999 (1.22842 pix)	5.6 million
RGS	37	379	99	355277	9.75 hours	66	13.75 hours	0.489 mm/pix	0.120506 (0.326652 pix)	0.299987 (1.76656 pix)	4 million

Table 5. Summary of model properties and quality (KPFS = author, EYC = consistent student, and RGS = random graduate students). See Appendices G, H, I for models.

Level 1 Model Summary of Results											
	Photo collection time (mins)	*Total No. Photos*	*Photo Alignment Percentage*	*Tie points*	*Time to Align Photos*	*Parameters Reached - Percent*	*Time to Dense Cloud*	*Ground Resolution*	*RMS reprojection error*	*Max reprojection error*	*No. points - Dense Cloud*
KPFS	40	372	100	329800	9.5 hours	66%	16 hours	.503 mm/pix	0.125705 (0.258303 pix)	0.309981 (1.38514 pix)	3.3 million
EYC	41	383	73	656522	10.75 hours	66	12 hours	n/a	.151021 (.492126 pix)	.726999 (31.437 pix)	3.1 million
RGS	100	375	99	384580	10.5 hours	66	11 hours	0.496 mm/pix	.125516 (0.261461 pix)	.310452 (1.34735 pix)	3.2 million

Table 6. Summary of model properties and quality (KPFS = author, EYC = consistent student, and RGS = random graduate students). See Appendices J, K, L for models.

Level 2 Model Summary of Results											
	Photo collection time (mins)	*Total No. Photos*	*Photo Alignment Percentage*	*Tie points*	*Time to Align Photos*	*Parameters Reached - Percent*	*Time to Dense Cloud*	*Ground Resolution*	*RMS reprojection error*	*Max reprojection error*	*No. points - Dense Cloud*
KPFS	37	339	99.7	388169	8.5 hours	33	15.5 hours	0.54 mm/pix	0.113715 (0.265695 pix)	0.299997 (1.97194 pix)	3.5 million
EYC	32	346	100	436150	9.25 hours	33	18.75 hours	0.571 mm/pix	0.122484 (0.280951 pix)	0.320373 (1.90444 pix)	4 million*
RGS	40	340	100	386541	8 hours	33	15.75 hours	.565 mm/pix	0.115294 (0.267484 pix)	0.300124 (2.04486 pix)	3.3 million

*estimated due to error in clipping point cloud

Average root mean squared error of all models was 0.126 (0.297 pixels), which shows that it was possible to obtain submillimeter accuracy for all models produced. Detailed presentations for each model can be found in Tables 4-6.

Hand Mapping

Hand mapping times varied between levels and subjects being mapped. For the surface and level 1, all six units were mapped by pairs of graduate students. All students were familiar with archaeological mapping techniques and for the first two levels of mapping, it took approximately 45 minutes to 1 hour to map each unit. Figure 15 shows the scanned surface maps for all six units. Unit 0N 0E is the southwestern unit. As can be seen, there is not a standard symbology for the map, and features which should extend between units do not line up properly. The map produced from tracing the features seen on the orthomosaic of the surface model (Figure 16) has accurate features and consistent symbology. The digitally produced map also took only one person a half hour to make, as opposed to eight graduate students over 1 hour per unit.

For level 2, when the skeletal material was fully uncovered, only the center two units were hand mapped (0N, 1E and 1N, 1E). This was primarily due to time constraints, as it took approximately 2 and a half hours to map each unit (5 hours total) by pairs of experienced graduate students. Digitally, the author was able to map the entire grave at level 2 within 2 hours.

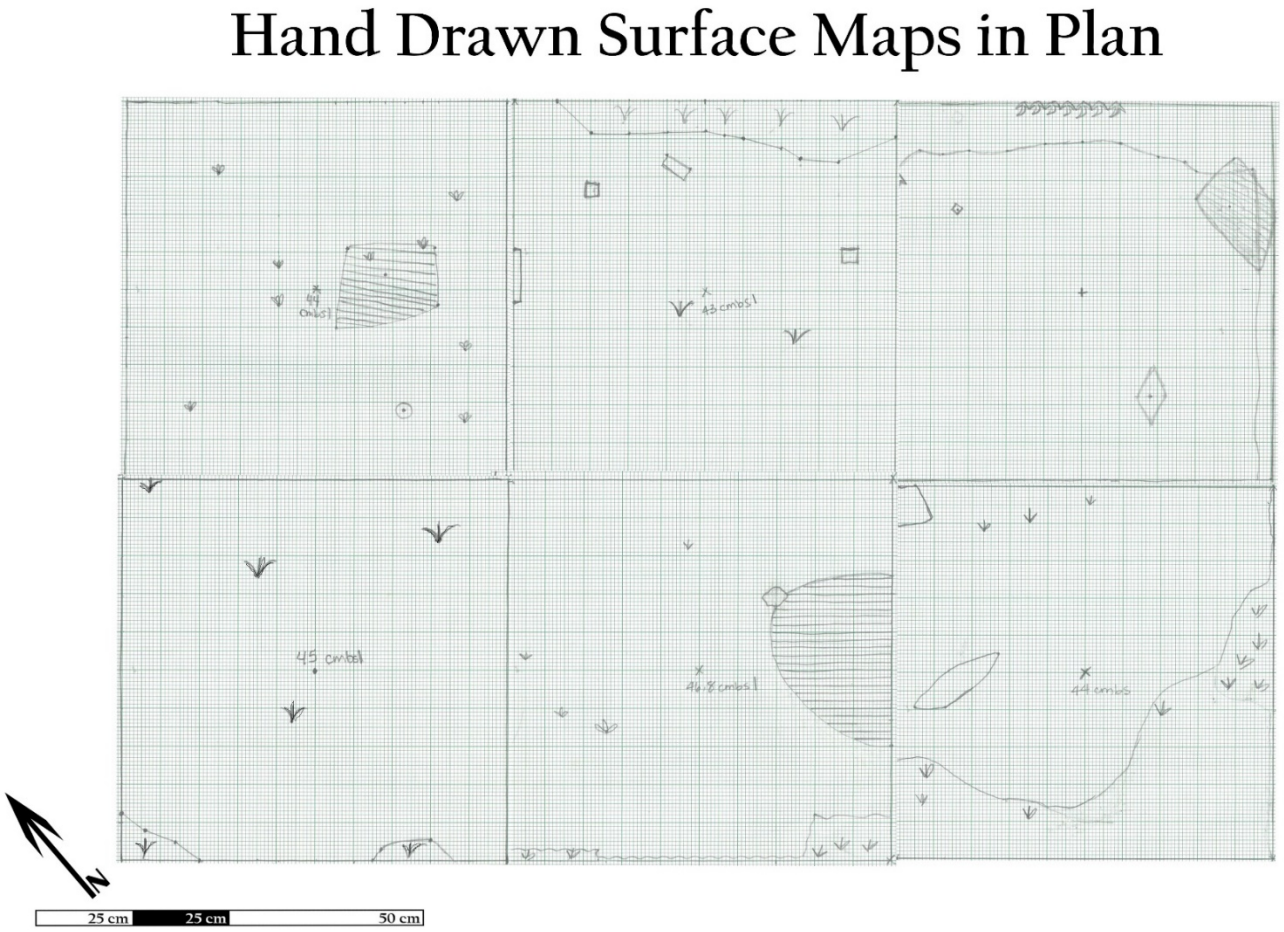

Figure 15. Scan of hand drawn maps stitched together. Notice inconsistencies between units and symbology.

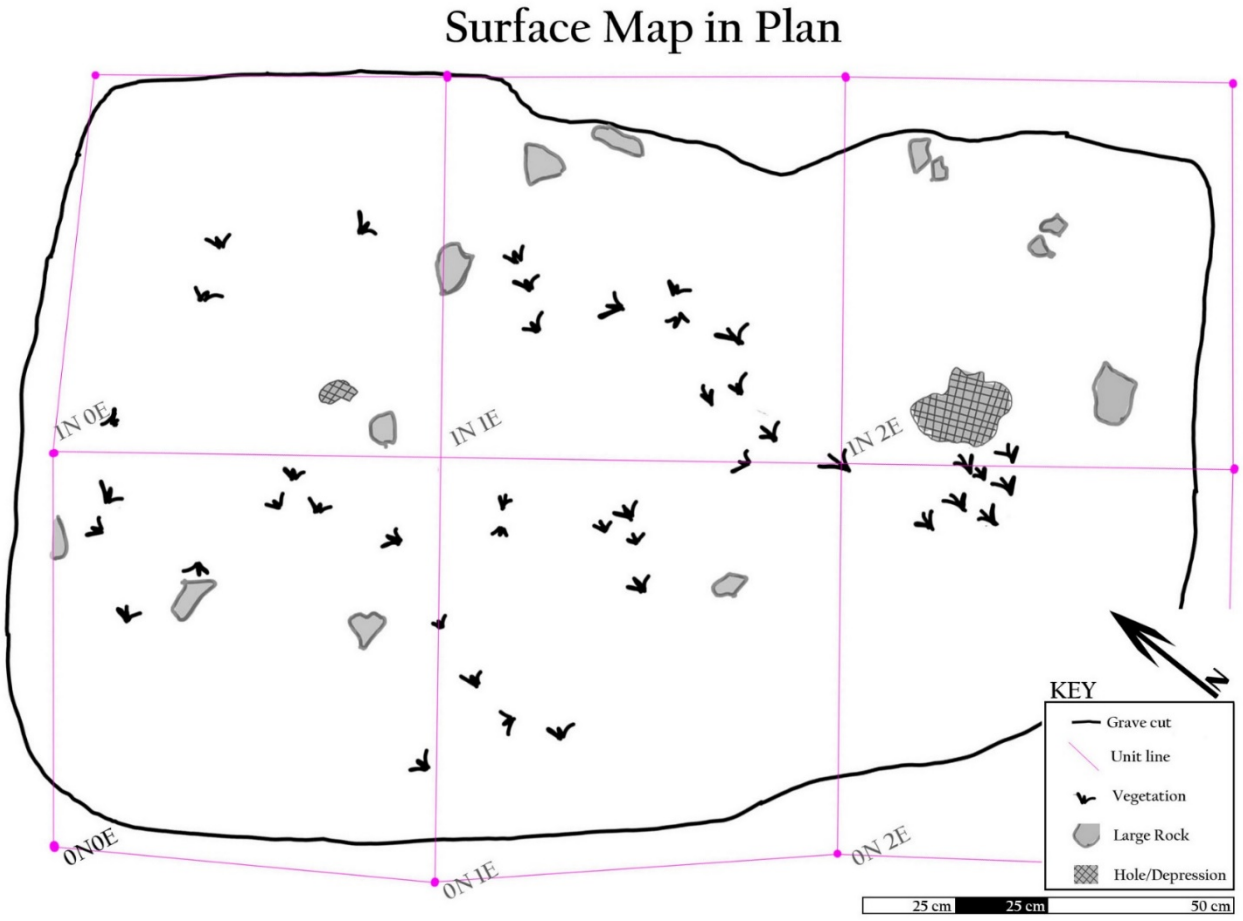

Figure 16. Digitally traced map from orthomosaic of surface.

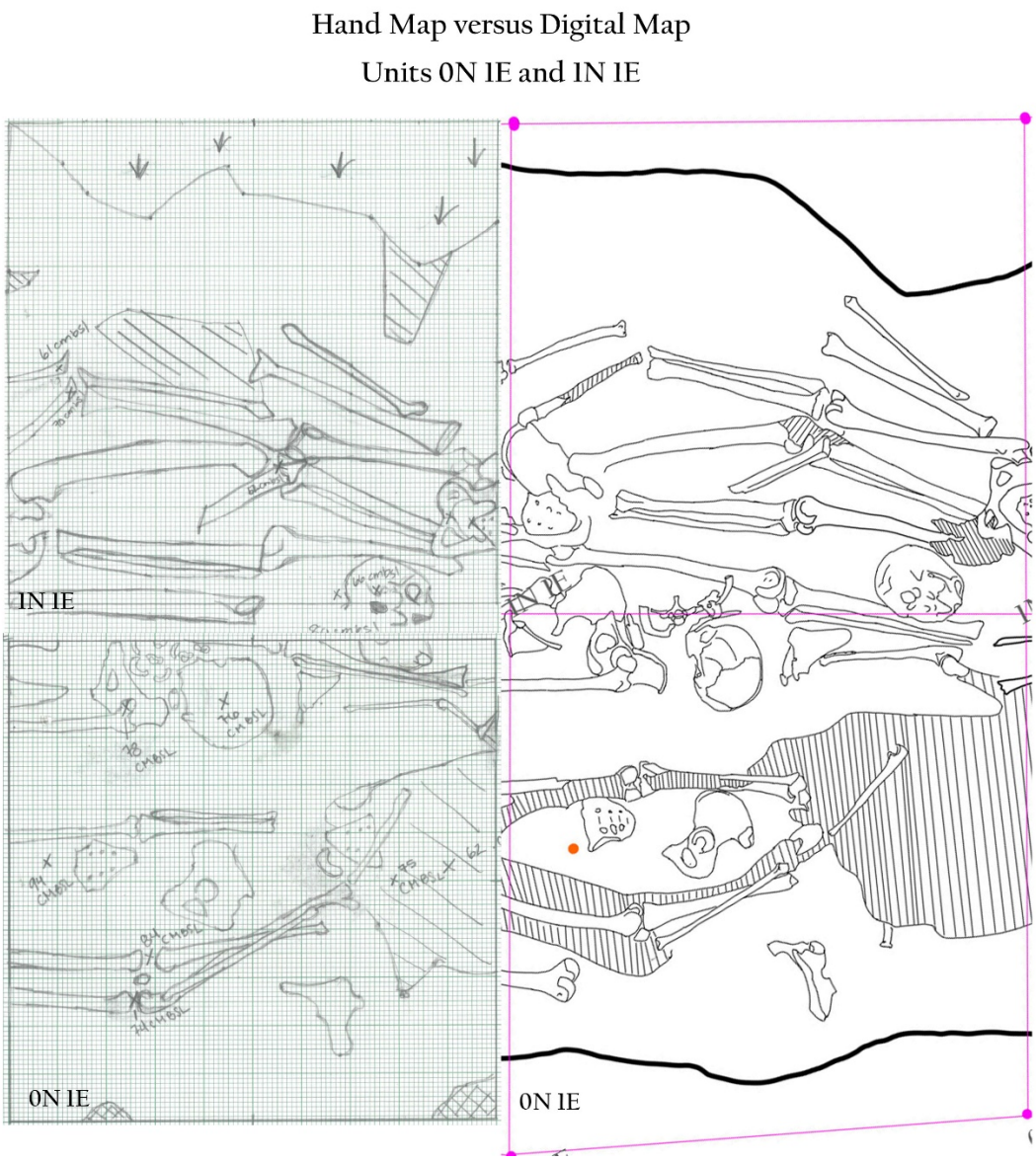

Figure 17. Side by side comparison of hand drawn map versus digitally drawn map. See Figure 20 for complete digital map.

Total Station Mapping

All total station mapping was completed by the author. Two methods were used for data point collection, a minimal method and a detailed method. Minimal data point collection was completed by taking points on the cranium, scapulae, elbow joint, wrist joint, sacrum, proximal femur, distal femur, and distal tibia (Figure 18). The minimal method was used for D46-2016, D58-2016, and D59-2016. The detailed method included taking several points on the skull, on proximal and distal ends of each bone, on each visible vertebra (Figure 19). This method was used for D41-2016 and D61-2016. The time to collect points is reported in Table 7. On average, the minimal method took 15 minutes, while the detailed method took 64 minutes. The time to collect detailed points on D41-2016 was very different than the time needed to collect points on D61-2016. The difference may be due to articulated versus scavenged remains.

Table 7. Time to collect data points using total station.

TS - Time to Collect Data Points by Donor		
Donation Number	*Method*	*Total Time*
D41-2016	detailed	48 minutes
D46-2016	minimal	14 minutes
D58-2016	minimal	12 minutes
D59-2016	minimal	19 minutes
D61-2016	detailed	80 minutes

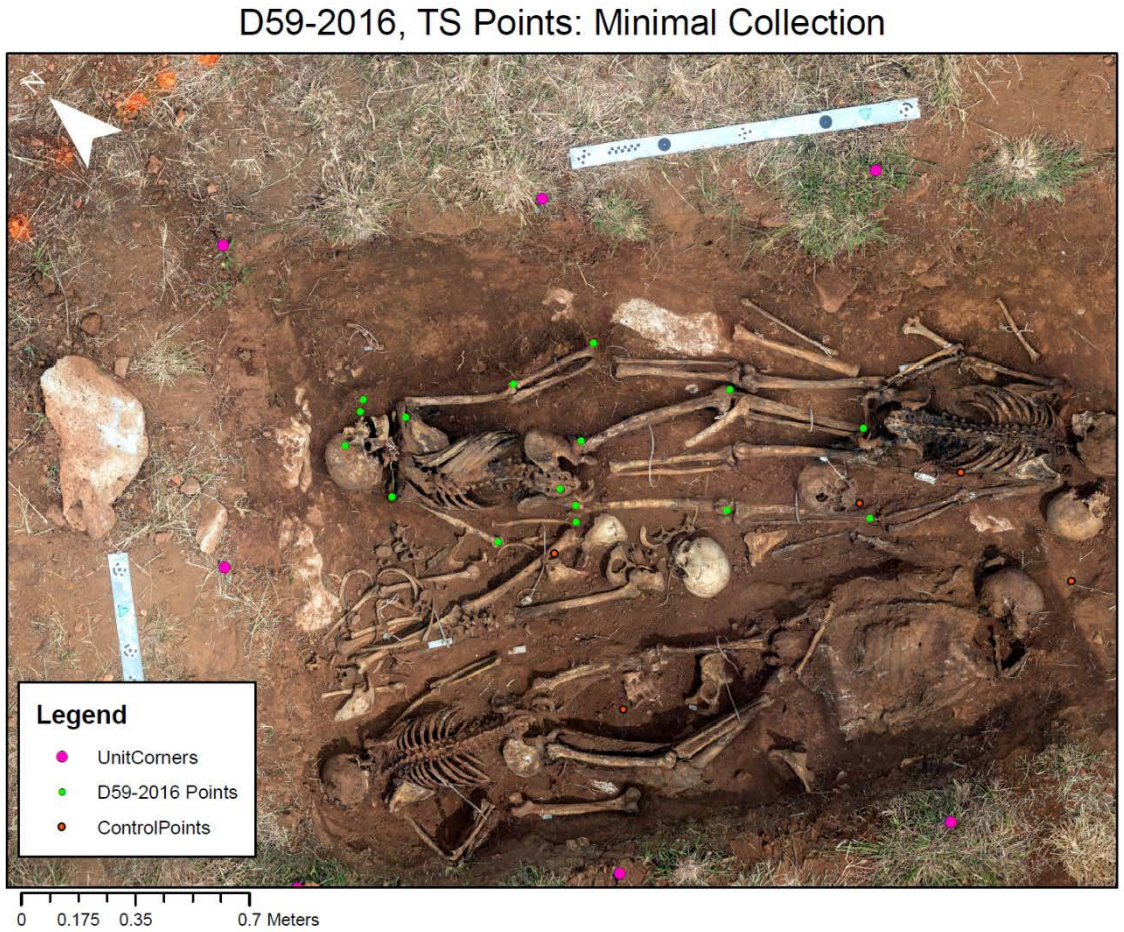

Figure 18. Map showing minimal point collection on D59-2016.

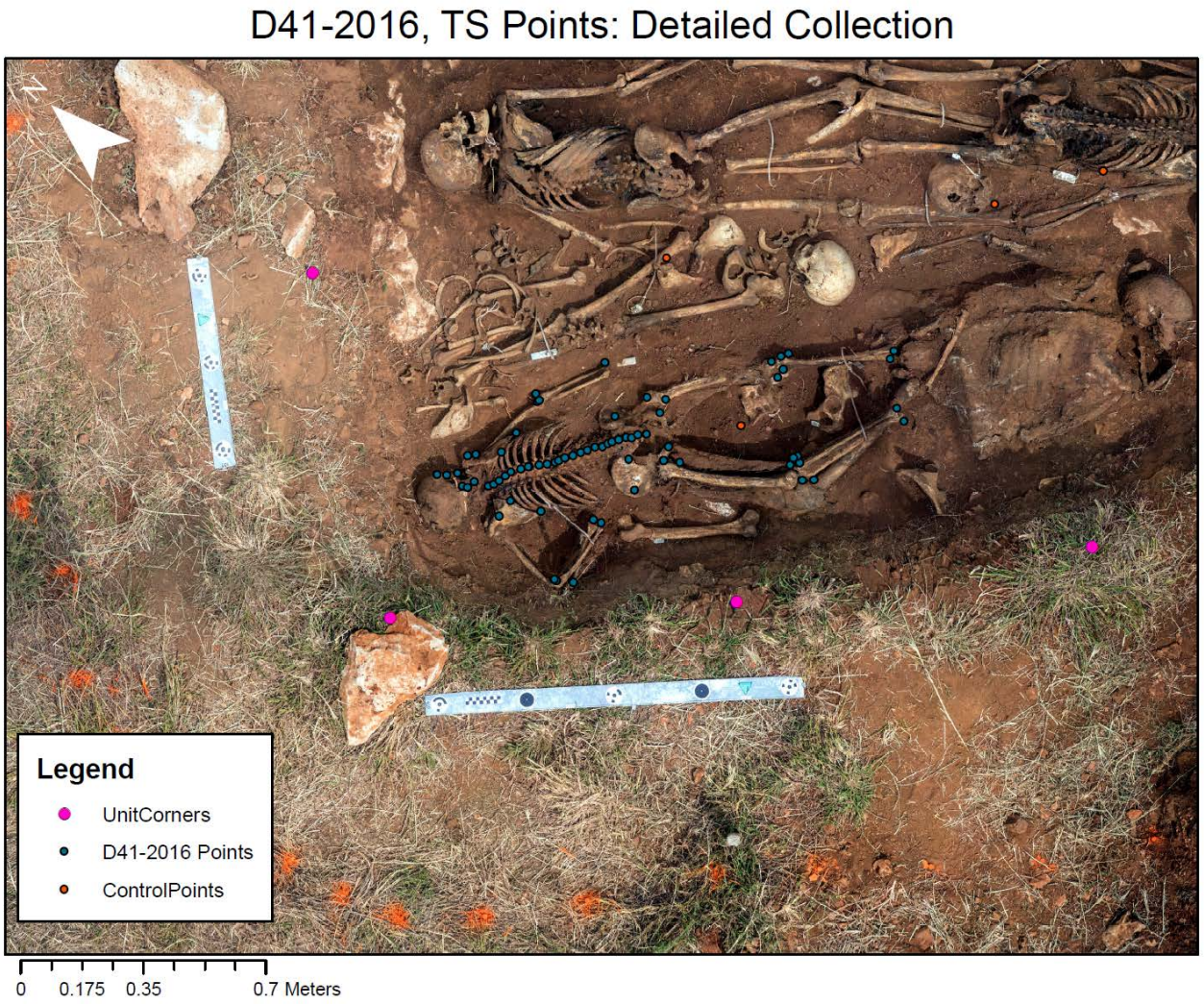

Figure 19. Map showing detailed point collection method on D41-2016.

Digital versus Physical Measurements

For all individuals and disarticulated skeletal elements (excluding D59-2016 due to lack of decomposition), measurements were taken traditionally (on physical, cleaned and processed, post-excavation bones). Measurements were also completed within the *in situ* SfM model and are referred to here as digital measurements. The full suite of physical measurements possible with available lab equipment included a modified selection of Howell's for craniometrics and a modified selection of Zobeck's for postcranial metrics. A comprehensive list of all possible measurements is included in Appendix C.

Given that physical measurements were in some cases not possible or limited, the average number of modified Howell's and Zobeck's physical cranial and postcranial measurements which could be taken of the complete donors was 98.25%.

The average number of modified Howell's and Zobeck's cranial and postcranial measurements taken digitally *in situ* was 29%. Digital measurements were possible less of the time due to constraints of what skeletal features were viewable within the *in situ* model, which were related to placement of donors, placement of DSEs, photo collection strategies, and factors related to excavation protocols. When comparing the complete individuals to the disarticulated skeletal elements (DSEs), the DSEs had a higher number of measurements able to be taken, with complete individuals' average percentage of possible digital measurements was 25%, whereas for the DSEs the average percentage of possible digital measurements was 43%.

The results of the statistical tests report that for the 239 Wilcoxon signed rank tests run, only 3 had a result which was statistically significant at the alpha = 0.95 level.

The Wilcoxon signed rank tests tested if the digital and physical skeletal measurements from the *in situ* model were significantly different from each other. These results support the null hypothesis of this test that the two groups are from the same population. In other words, the digital and physical measurements are not significantly different from each other in 98.8% of the tests run. Summarized in Tables 8-12 are the specific results from each individual. Figures 18 and 19 show the process of measuring GOL for D61-2016.

Figure 20. Selecting glabella with measure tool in Agisoft, indicated with white arrow.

Figure 21. Selecting opisthocranion to measure GOL, indicated with white arrow.

Table 8. Summary of total measurements possible physically and digitally and overview of the results of Wilcoxon tests. Non-paired post-cranial elements were included in the count of the right side.

D41-2016 Measurements Summary					
	Meas. Possible	*Percent Trad. Physicall Meas. Taken*	*Percent Digital Meas. Taken*	*Number of Wilcoxon tests Run*	*Number of significant Wilcoxon tests α=.95*
Cranial	36	97	14	5	0
Mandibular	7	100	14	1	0
Left Post-Cranial	56	98	25	13	0
Right Post-Cranial	66	100	29	19	0
Overall	165	99	20	38	0

Table 9. Summary of total measurements possible physically and digitally and overview of the results of Wilcoxon tests. Non-paired post-cranial elements were included in the count of the right side.

D46-2016 Measurements Summary					
	Amount Possible	*Percent Trad. Physical Meas. Taken*	*Percent Digital Meas. Taken*	*Number of Wilcoxon tests Run*	*Number of significant Wilcoxon tests a=.95*
Cranial	36	97	33	12	1
Mandibular	7	100	43	3	0
Left Post-Cranial	59	100	34	20	0
Right Post-Cranial	66	100	27	18	1
Overall	168	99.25	34	53	2

Table 10. Summary of total measurements possible physically and digitally and overview of the results of Wilcoxon tests. Non-paired post-cranial elements were included in the count of the right side.

D59-2016 Measurements Summary					
	Amount Possible	*Percent Trad. Physical Meas. Taken*	*Percent Digital Meas. Taken*	*Number of Wilcoxon tests Run*	*Number of significant Wilcoxon tests a=.95*
Cranial	36	100	28	10	0
Mandibular	7	100	43	3	0
Left Post-Cranial	59	100	12	7	0
Right Post-Cranial	66	100	12	10	0
Overall	168	100	24	30	0

Table 11. Summary of total measurements possible physically and digitally and overview of the results of Wilcoxon tests. Non-paired post-cranial elements were included in the count of the right side.

D61-2016 Measurements Summary					
	Amount Possible	*Percent Trad. Physical Meas. Taken*	*Percent Digital Meas. Taken*	*Number of Wilcoxon tests Run*	*Number of significant Wilcoxon tests a=.95*
Cranial	36	100	42	14	1
Mandibular	7	100	0	0	n/a
Left Post-Cranial	54	100	28	15	0
Right Post-Cranial	60	100	25	15	0
Overall	157	100	24	44	1

Table 12. Summary of total measurements possible physically and digitally and overview of the results of Wilcoxon test.

Disarticulated Skeletal Elements Measurements Summary						
	Elements	*Measur. Possible*	*Percent Traditional Meas. Taken*	*Percent Digital Meas. Taken*	*Number of Wilcoxon tests Run*	*Number of significant Wilcoxon tests a=.95*
D07-2015	Sacrum	3	100	100	3	0
	Innominate	2	100	50	1	0
	Humerus	7	100	29	1	0
	Lumbar Vertebra	1	100	0	0	n/a
D19-2014	Clavicle	3	100	100	3	0
	Mandible	7	100	86	6	0
	Scapula	8	100	63	5	0
	Radius	5	80	40	2	0
D36-2015	Scapula	8	100	63	5	0
	Tibia	7	100	29	2	0
	Fibula	2	100	50	1	0
	Cranium	36	100	50	18	0
D09-2015	Femur	15	100	53	8	0
	Fibula	2	100	100	2	0
D01-2015	Clavicle	3	100	66	0	n/a
D44-2012	Atlas	1	0	0	0	n/a
	Axis	1	100	0	0	n/a
D15-2016	Innominate	2	100	0	0	n/a
	Tibia	7	86	0	0	n/a
	Thoracic Vertebra	1	100	0	0	n/a
D46-2014	Ulna	10	90	40	4	0
	Cranium	36	100	36	13	0
	Overall	167	93	43	74	0

IV. DISCUSSION

To assess ease of learning photogrammetry, several comparisons were made. Photo collection time was a useful metric to look at, and the results show that total time did not vary significantly between experts and non-experts. While one student took a longer time than the others at 100 minutes to collect photos, this time is still faster than the total time to complete traditional documentation including hand maps, total station data collection, and traditional photography. Additionally, all the data collected in the traditional documentation process can be gathered or created from the photogrammetric models. Utilizing a photogrammetric workflow eliminates redundancies in the collection of data and can speed up work. If documentation is completed more quickly, excavation can proceed sooner. Additionally, faster documentation could allow more precise excavation in complex burials by freeing up significant amounts of time that would otherwise be spent on hand-mapping or total station mapping.

An essential step in the process to allow the creation of high quality models was laying out photo positions. This was only done for the dome model, though it would be possible to lay out start and end points for the strips of the plane model easily. The dome model positions were laid out in approximately 2 hours using a compass, to ensure that no position had more than a 10-degree change. Having the strip beginning and ending points for the plane model could have further standardized the quality of the models created by the various skill levels and ensured complete coverage of the grave. However, this was not a large issue and none of the models had gaps which affected the area containing human remains.

When comparing the map products produced by hand-mapping in the field and from orthomosaics produced from the SfM models, the digitally-created maps contain more detail and took less time and less personnel to produce. A highly detailed map of the entire exposed grave was completed in two hours by the author from an orthomosaic (see Figure 20), whereas to map two units of the same level in the field, it took five graduate students 5 hours total. Additionally, by tracing the orthomosaic to create a digital map, subjectivity and errors caused by parallax and measurement error are removed from the mapping process, creating a more accurate map product. While using photogrammetry cannot completely replace using a total station or other geodesic equipment in terms of locational data, such as coordinates, it can reduce the need for detailed point collection. At least three GPS coordinates or point locations should still be collected to georeference the models, but it is not necessary to collect as many points as were collected on D41-2016 and D61-2016. Even the minimal data point collection strategy used on the other articulated donations could be simplified if the SfM models are precise enough. Finally, less accuracy may be required of the geodesic equipment, total station or other GPS, if calibrated or highly precise scale bars are used because the model could use exclusively the scale bars to scale the model and the locational data only to georeference. This would likely reduce the costs of operation of geodesic equipment and reduce the need for specialized technicians.

Ease of use was quantified by comparing the results of the models between the expert, the consistent graduate student, and the random graduate students. While processing of all models was completed by an expert, the results show that experts and non-experts alike can collect photos which will create models with similar rates of error. All the models fell

within acceptable error parameters as defined by Matthews (2008). Root mean squared (RMS) reprojection error is the primary measure which was used to determine if models were above or below a certain quality threshold, with the desired RMS reprojection error being around 0.12. The level 1 model completed by the consistent graduate student is the only model which did not meet this parameter as it had an RMS reprojection error of 0.15. At initial alignment of photos, only 73% of the photos aligned, though the reason is not known. After a second alignment was done, 100% of the photos were aligned. The initial trouble of the software to register the photographs, possibly due to improper endlap, sidelap, or discontinuous photo collection, may be part of the reason the RMS reprojection error was slightly higher in this case than the error of other models. Further care in collecting photos and ensuring good quality would have likely have prevented this.

The second focus of this research was to determine if accurate skeletal measurements could be collected from within the digital *in situ* models. The definition of photogrammetry provided by Thompson, et al. (1966) emphasizes the purpose of the entire endeavor: to produce measurements. If accurate measurements are not possible from within digital models, then what is being produced are 3D visualizations, not photogrammetric models. Based on the results of this project, if the photogrammetric data collection procedures outlined above are followed, accurate measurements are possible.

In total, 239 Wilcoxon signed rank tests were run to compare the physical and digital data for each skeletal measurement. Three of these tests had statistically significant results.

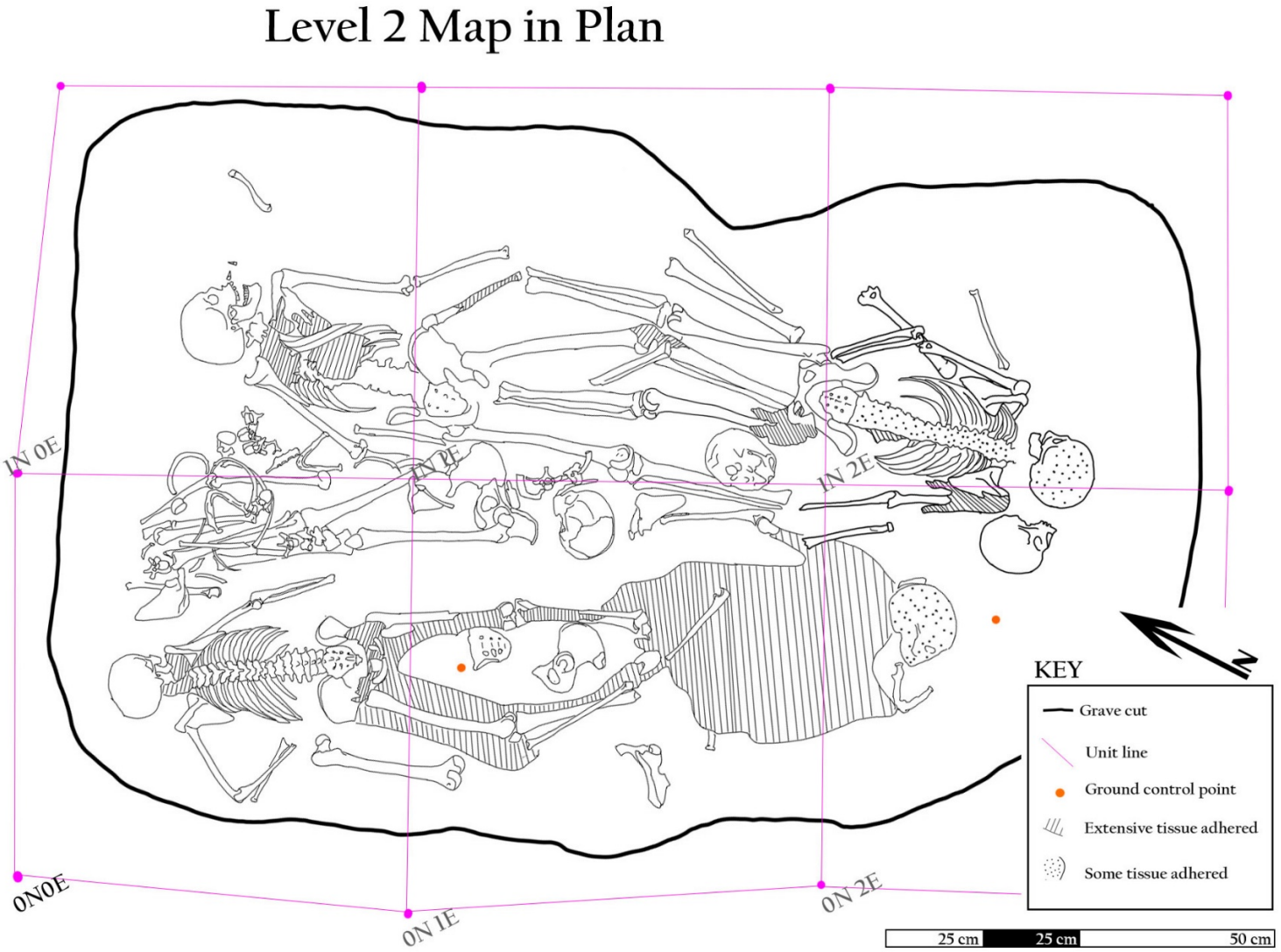

Figure 22. Level 2 map produced by tracing orthomosaic.

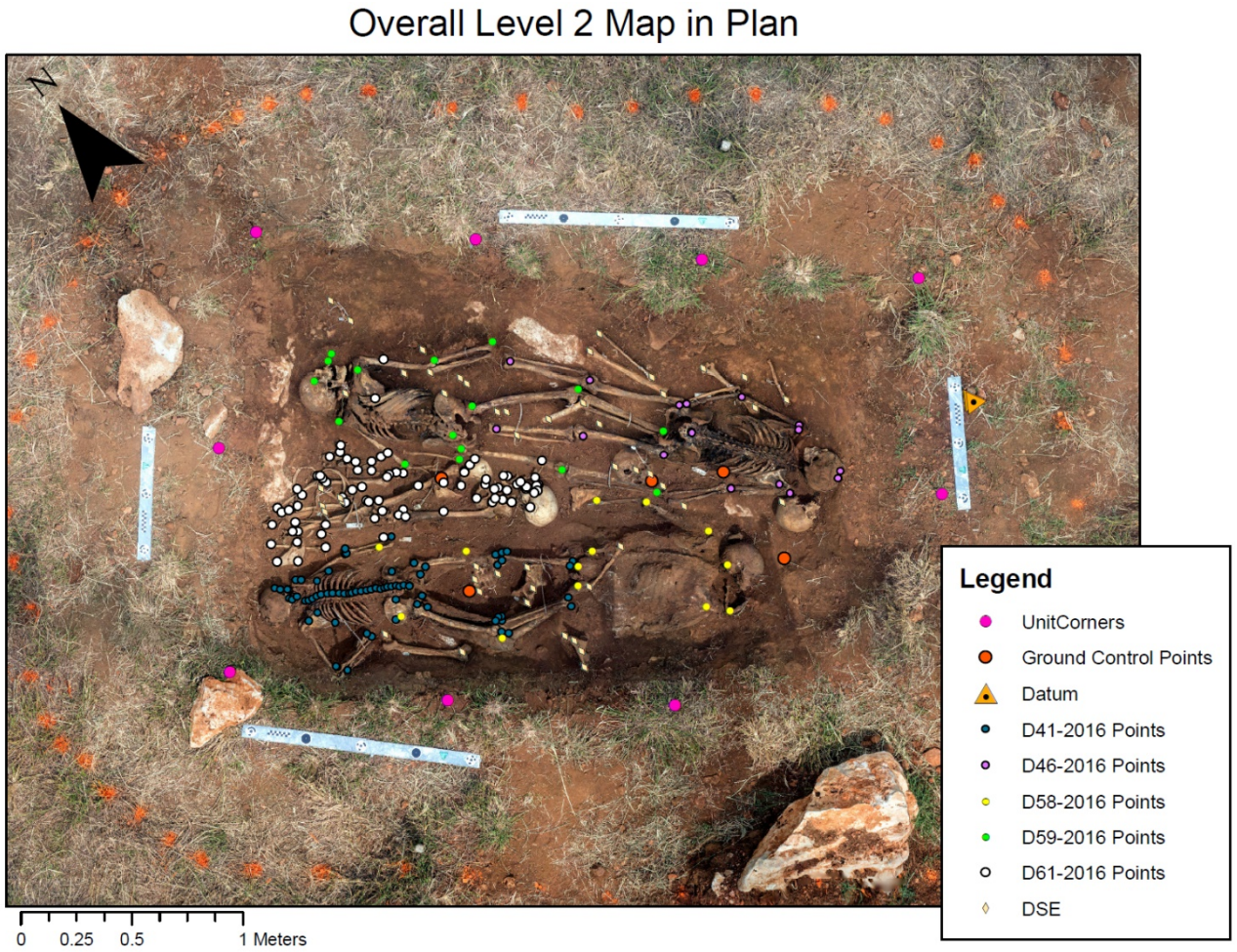

Figure 23. Overall level 2 map with data points from total station.

Wilcoxon signed rank tests were performed to compare the physical data numbers to the digital data numbers for each measurement which was able to be taken in both methods. The null hypothesis of the Wilcoxon signed rank test is that the two samples come from the same population. If the test statistic, W and p-values, are not significant, you cannot reject the null hypothesis. The results of this statistical analysis show that accurate skeletal measurements can be taken from within the digital *in situ* models, directly refuting Baier and Rando's (2016) findings.

The primary limit on digital *in situ* measurements was related to the position of elements within the grave. Physically, in both the field and in the laboratory, measurements are almost always possible. Within the digital *in situ* model, not all sides of a bone will be visible since they are still encased in burial matrix to some degree. This fact, for most of the elements included in this thesis, significantly limited the number of skeletal measurements possible. The measurements possible are directly related to the positioning of the body. A potential option to explore in the future would be integrating lab-derived SfM models of individual elements into the *in situ* models, which could enable all measurements to be taken, because if a complete model of a bone is integrated, the bone could then be rotated within the *in situ* model to adequately view all features for measurement.

The possibility of digital measurements was also different for articulated versus disarticulated skeletal elements. In the articulated individuals, necessary landmarks or features were often obscured by other skeletal features (e.g., the head of the femur still being articulated in the acetabulum). For this specific project, adhered tissue also limited the measurements possible. With further time for decomposition to occur, as would be

expected in a mass grave or clandestine burial older than the 3-month time-frame used in this study, this would likely not be an issue.

The final question this research sought to answer was whether a set of best practices for using photogrammetry for excavation with human remains could be developed to maximize the potential of the photogrammetric models. This research showed that this could be developed for this purpose, and the author is working on developing a detailed protocol and workflow guidance for this use. For now, in order to collect photogrammetric data for buried human remains, several best practices can be followed:

1. Pre-planning of photo locations should be completed for either the plane or dome model, depending on the size of the area to be documented
2. Photos should be collected to create both a plane and a dome model. A monopod or tripod and remote shutter should be used to get the best photos
    a. When the situation permits, close-up photos can greatly enhance the outcome of the final model in terms of visible detail and texture
3. Recommended equipment includes: camera, monopod or tripod with varying heights, compass, nails, computer which meets specifications, large external hard drive, scale bar or GPS points.
4. Between four and six ground control points should be shot in with known coordinates to georeference the model
5. For buried human remains, skeletal elements should be exposed to the maximum extent possible

The exposure of as much skeletal material as possible is crucial to maximize the number of measurements within the digital *in situ* model. Pedestaling can be done, but the goal should be to remove all soil matrix not essential to maintaining structural integrity. If remains are fleshed, the same protocol should be followed to maximize exposure. However, this research serves as a basis and an optimal case for using photogrammetry. Deep burials with steep walls would limit the ability of photos to capture all views of remains, though it would still be possible to collect some photos, particularly for plane models. Additionally, highly commingled remains with many levels would complicate the later production of models and necessitate strict photo collection strategies. Further research could explore the possibilities and limits of photogrammetry in relation to documenting human remains at fresh, decomposing, and skeletonized stages.

V. CONCLUSIONS

This research sought to explore how Structure from Motion photogrammetry can best be applied to documenting buried human remains. More specifically, it sought to determine if accurate skeletal measurements could be taken from within the digital *in situ* models. 3D documentation is increasingly being incorporated into many different archaeological research projects, however photogrammetry is unique in its low price point when compared to other methods like terrestrial laser scanning or computed tomography. The shortcoming of photogrammetry is the delay in the ability to visualize collected data immediately, however, it is possible to process models on lower resolutions in order to have preliminary results and check the data before the next field day.

From the results of this study, it is possible to conclude that photogrammetry is an inexpensive option which is easy to learn. Non-experts, after a brief introduction and instructions from an experienced photogrammetrist, can collect the photos necessary to produce highly accurate models. These models can be taken as often as desired and can aid in recording the destructive processes inherent in archaeological and forensic excavations. Additionally, while it was not directly tested in this study, there is no evidence that non-experts would be unable to complete the model processing and create highly accurate models as well. Forensic anthropology and forensic archaeological investigations can benefit highly from incorporating this technology into their workflows. It saves time when compared to traditional documentation techniques and requires no additional equipment, except perhaps a monopod/tripod. When considering sites where

access needs to be limited for security or sensitivity issues, photogrammetry can reduce the number of skilled technicians necessary to complete proper documentation of the site.

It is important to consider the role of documentation for forensic anthropologists and archaeologists in preserving, in reproducible form, all aspects of crime scenes and cultural heritage sites. Structure from Motion photogrammetry is a technology which allows exactly that. Forensic anthropologists are often called upon to document and analyze some of the worst aspects of human activity, including murder, genocide and mass disasters. To effect change and create accurate understandings of these events in both the present and the past, both pleasant and unpleasant aspects of human activity must be documented. In mass disasters, exhuming and identifying the dead effectively is the top priority. Reproducing the scene can aid in courtroom and legal settings, and assist in learning to deal with similar situations in the future. Accessible technology such as photogrammetry can help maximize the efficiency and efficacy of forensic excavation and recovery, helping victims and communities affected by human rights abuses or mass disasters via a quick, inexpensive, and accurate technology that should be part of every forensic anthropologist's toolkit.

APPENDIX SECTION

APPENDIX A: BLANK PHOTO LOG SHEET

Photo Log

K. Flor-Stagnato Thesis
Page of

Date	Beginning Number	ISO	Aperture	Focal Length	Shutter Speed	Time Start	Project Type	Subject	End Number	End Time	SD Card	Initials
							Pln / Do					
							Pln / Do					
							Pln / Do					
							Pln / Do					
							Pln / Do					
							Pln / Do					
							Pln / Do					
							Pln / Do					
							Pln / Do					
							Pln / Do					
							Pln / Do					
							Pln / Do					
							Pln / Do					
							Pln / Do					
							Pln / Do					
							Pln / Do					
							Pln / Do					
							Pln / Do					
							Pln / Do					
							Pln / Do					
							Pln / Do					
							Pln / Do					
							Pln / Do					
							Pln / Do					
							Pln / Do					

Processing Log

Subject		Level		Strat		Photographer
Plane Model						
Preprocessing						
Photo numbers						
Began		**Finished**				
Number of Strips:						
Strip Photo Numbers:		*Begin*	*End*	*Angle*		
	Strip 1					
	Strip 2					
	Strip 3					
	Strip 4					
	Strip 5					
	Strip 6					
Notes:						
	Import Photos					
		Camera Groups				
		Camera Calibration Groups				
	Align Photos					
		(high, generic, 60,000, 0, uncheck adaptive)				
		Tie points				
		projected points per photo				
		initial adjusted				
	Optimize					
	Gradual Selection					
		Reconstruction Uncertainty (10 but no more than half)				
		Number				
	Optimize					
		Projection Accuracy (2) no more than 1/2 selected				
			Actual reached			
	Optimize					
	Add Scale					
		TDS				
		CSBs				
	Settings					
		Tie point accuracy 0.1				
	Optimize					
		check k4, b1, b2, p3, p4				
	Save					
	Gradual Selection					
		Reprojection error - no more than 10 percent of points selected				
			Actual reached			
	Optimize					
	Gradual Selection					
		Reprojection error until 0.3				
			Actual reached			
	Optimize					
	SEUW ~1					
	Dense point cloud					
		Number of points				
		Error				
	Mesh					
		Number of polygons				

APPENDIX C: CRANIAL AND POST CRANIAL MEASUREMENTS

List of All Cranial Measurements Used						
No.	*Measurement*	*Abbreviation*		*No.*	*Measurement*	*Abbreviation*
1	Maximum Length from Glabella	GOL		**23**	Interorbital breadth	DKB
2	Maximum Length from Nasion	NOL		**24**	Simotic chord	WNB
3	Cranial Base Length	BNL		**25**	Bimaxillary breadth	ZMB
4	Basion to Bregma	BBH		**26**	Bifrontal breadth	FMB
5	Maximum Cranial Breadth	XCB		**27**	Biorbital breadth	EKB
6	Maximum frontal breadth	XFB		**28**	Malar inferior	IML
7	Minimum Frontal Breadth	WFB		**29**	Malar max length	XML
8	Bizygomatic breadth	ZYB		**30**	Cheek height	WMH
9	Biauricular breadth	AUB		**31**	Bistephanic breadth	STB
10	Min. cranial breadth	WCB		**32**	Frontal chord	FRC
11	Biasterion breadth	ASB		**33**	Parietal chord	PAC
12	Basion-prostion length	BPL		**34**	Occipital chord	OCC
13	Nasion-prostion height	NPH		**35**	Foramen magnum length	FOL
14	Nasal height	NLH		**36**	Foramen magnum breadth	FOB
15	Bijugal breadth	JUB		**37**	Chin Height	
16	Nasal breadth	NLB		**38**	Body Height at Mental Foramen	
17	Ext. palate breadth	MAB		**39**	Body Thickness at Mental Foramen	
18	Ext. palate length	MAL		**40**	Bigonial Diameter	
19	Mastoid height	MDH		**41**	Bicondylar Breadth	
20	Mastoid breadth	MDB		**42**	Minimum Ramus Breadth	
21	Orbital height	OBH		**43**	Maximum Ramus Height	
22	Orbital breadth	OBB				

List of All Post-cranial Measurements Used							
No.	*Bone*	*Measurement*	*Abbrev.*	*No.*	*Bone*	*Measurement*	*Abbrev.*
1	Clavicle	Clavicle max length	CML	**34**	Ulna	Ulna olec-coronoid length	OCL
2		Clavicle A-P diam midshaft		**35**		Ulna A-P diam shaft	
3		Clav S-I diam midshaft		**36**		Ulna M-L diam midshaft	
4	Scapula	Scapula max height	SML	**37**		Ulna least circum shaft	ULC
5		Scapula max breadth	SMB	**38**	Sacrum	Sacrum anterior length	
6		Scapula spine length	SLS	**39**		Sacrum A-S breadth	
7		Scapula supraspinous length	SSL	**40**		Sacrum max breadth S1	
8		Scapula infraspinous length	ISL	**41**	Innominate	Innominate height	
9		Scap glenoid cavity breadth	GCB	**42**		Iliac breadth	
10		Scap glenoid cavity height	GCH	**43**	Femur	Femur max length	FML
11		Scap glenoid to inf angle	GIL	**44**		Femur bicondylar length	FOL
12	Sternum	Manubrium length		**45**		Femur trochanteric length	FTL
13		Mesosternum length		**46**		Fem subtroch A-P diam	APD
14		Stenebra 1 width		**47**		Fem subtroch M-L diam	MLD
15		Stenebra 3 width		**48**		Fem A-P diam midshaft	APS
16	Humerus	Humerus max length	HML	**49**		Fem M-L diam midshaft	MLS
17		Hum prox epiph breadth	BUE	**50**		Fem max vert diam head	VHD
18		Hum max diam midshaft	MDS	**51**		Fem max horiz diam head	HHD
19		Hum min diam midshaft	MDM	**52**		Fem A-P diam lat condyle	APL
20		Hum max diam head	MDH	**53**		Fem A-P diam med cond	APM
21		Hum epicondylar breadth	EBR	**54**		Fem epicondylar breadth	FEB
22		Hum least circum of shaft	LCS	**55**		Fem bicondylar breadth	BCB
23	Radius	Radius max length	RML	**56**		Fem min vert diam neck	VDN
24		Radius max diam head	RDH	**57**		Femur circum midshaft	
25		Radius A-P diam of shaft		**58**	Tibia	Tibia condylo-malle length	TML
26		Radius M-L diam of shaft		**59**		Tibia max br prox epiph	BPE
27		Radius neck shaft circum	MCS	**60**		Tibia max br dist epiph	BDE
28	Ulna	Ulna max length	UML	**61**		Tibia A-P diam nut for	APN
29		Ulna physiological length	UPL	**62**		Tibia M-L diam nut for	MLM
30		Ulna max br olecranon	BOP	**63**		Tibia position of nut for	CFL
31		Ulna min br olecranon	MBO	**64**		Tibia cirum at nut for	
32		Ulna max wd olecranon	WOP	**65**	Fibula	Fibula maximum length	BML
33		Ulna olec-radial notch	ORL	**66**		Fibula max diam midshaft	

APPENDIX D: Surface Model by Random Graduate Student

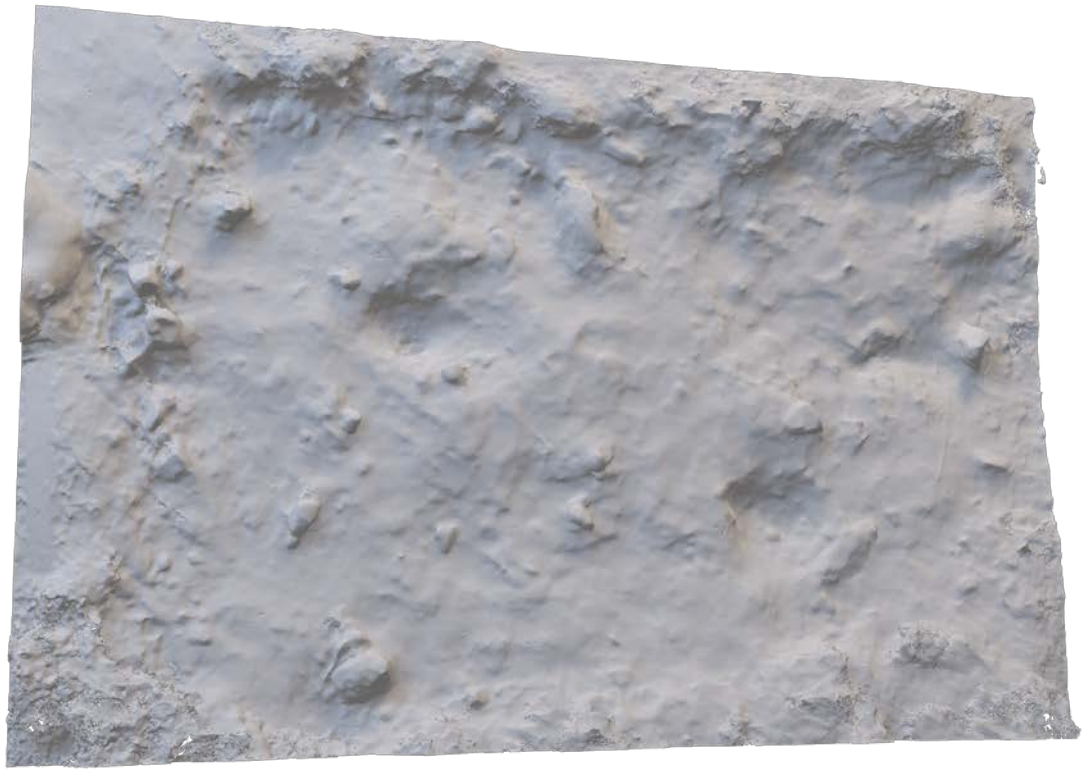

APPENDIX E: Surface Model Created by Consistent Graduate Student

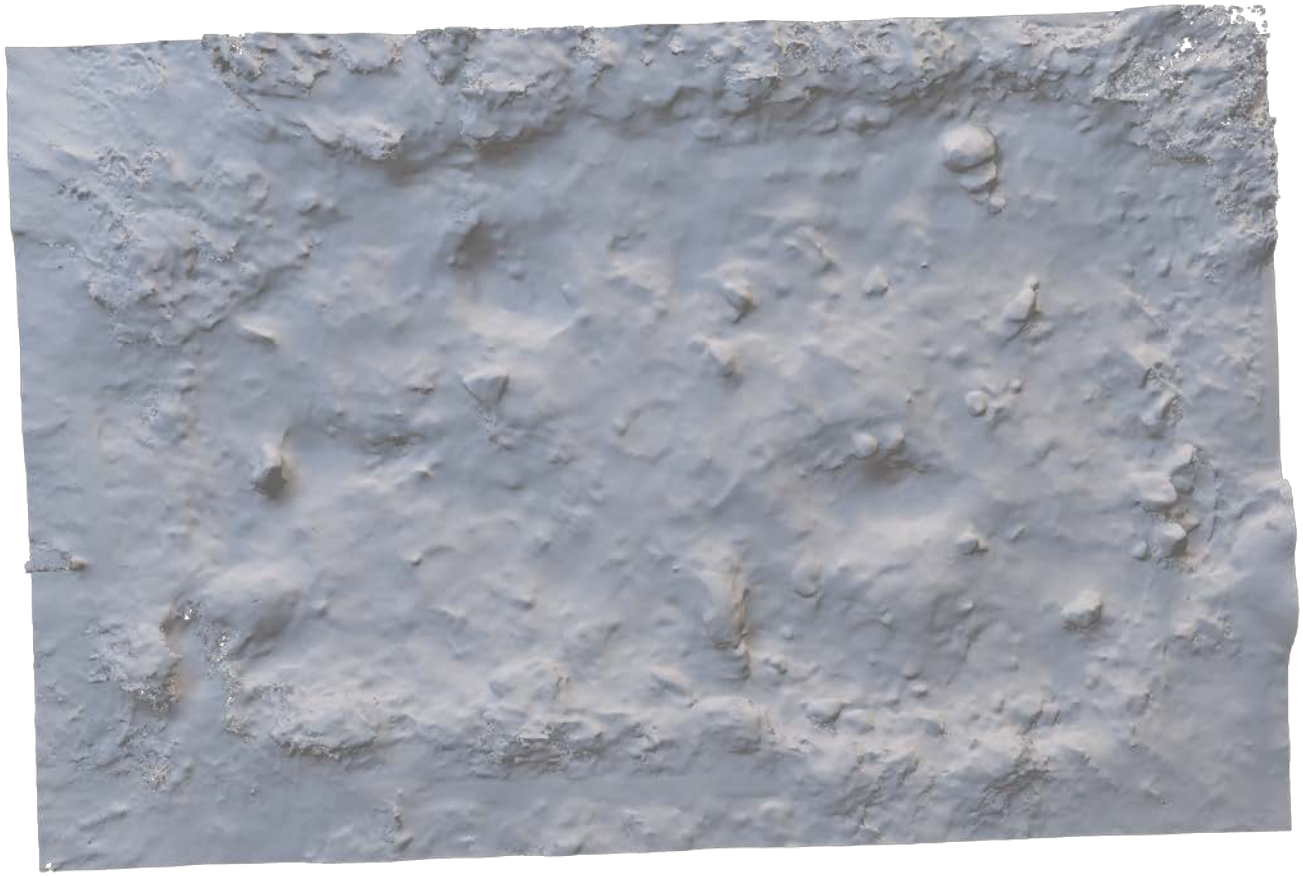

APPENDIX F: Surface Model by Author

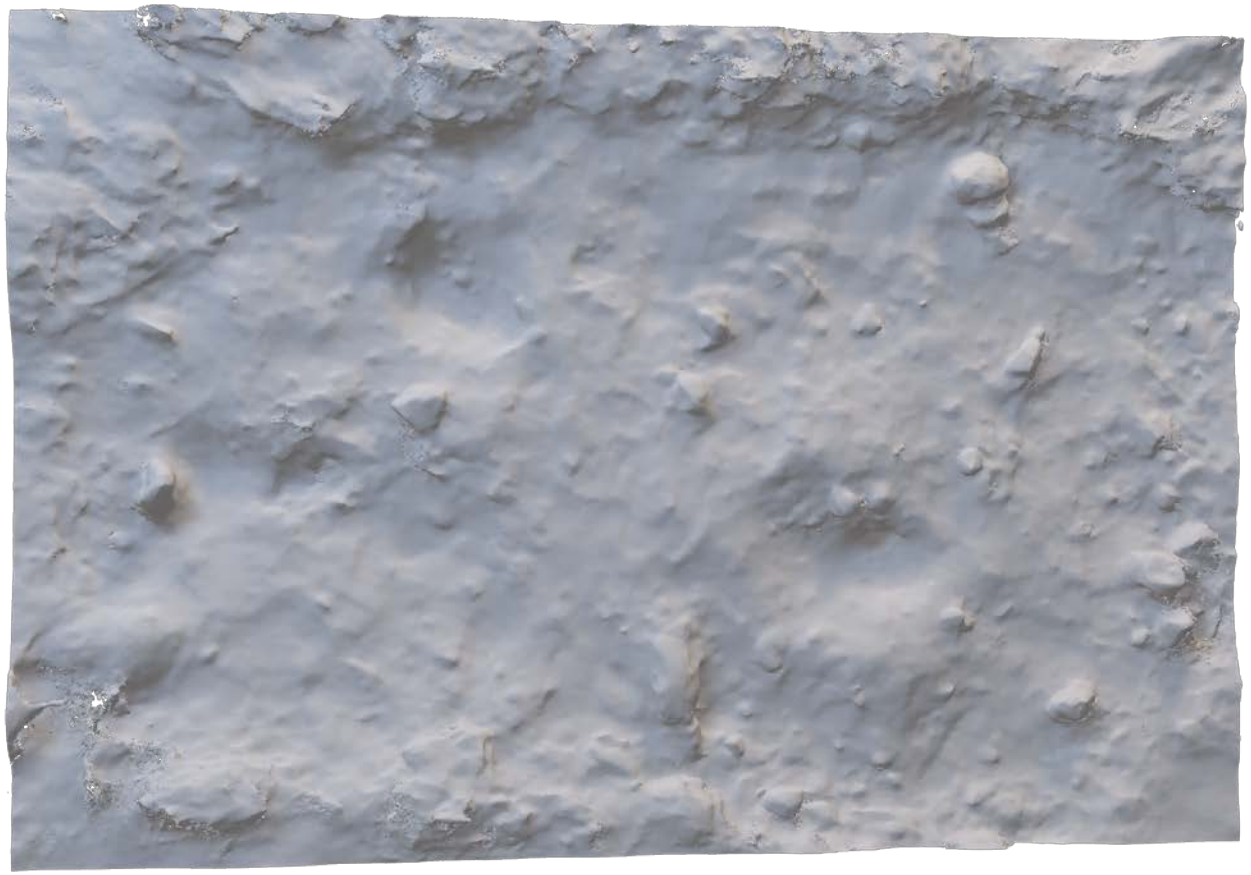

APPENDIX G: Level 1 Model by Random Graduate Student

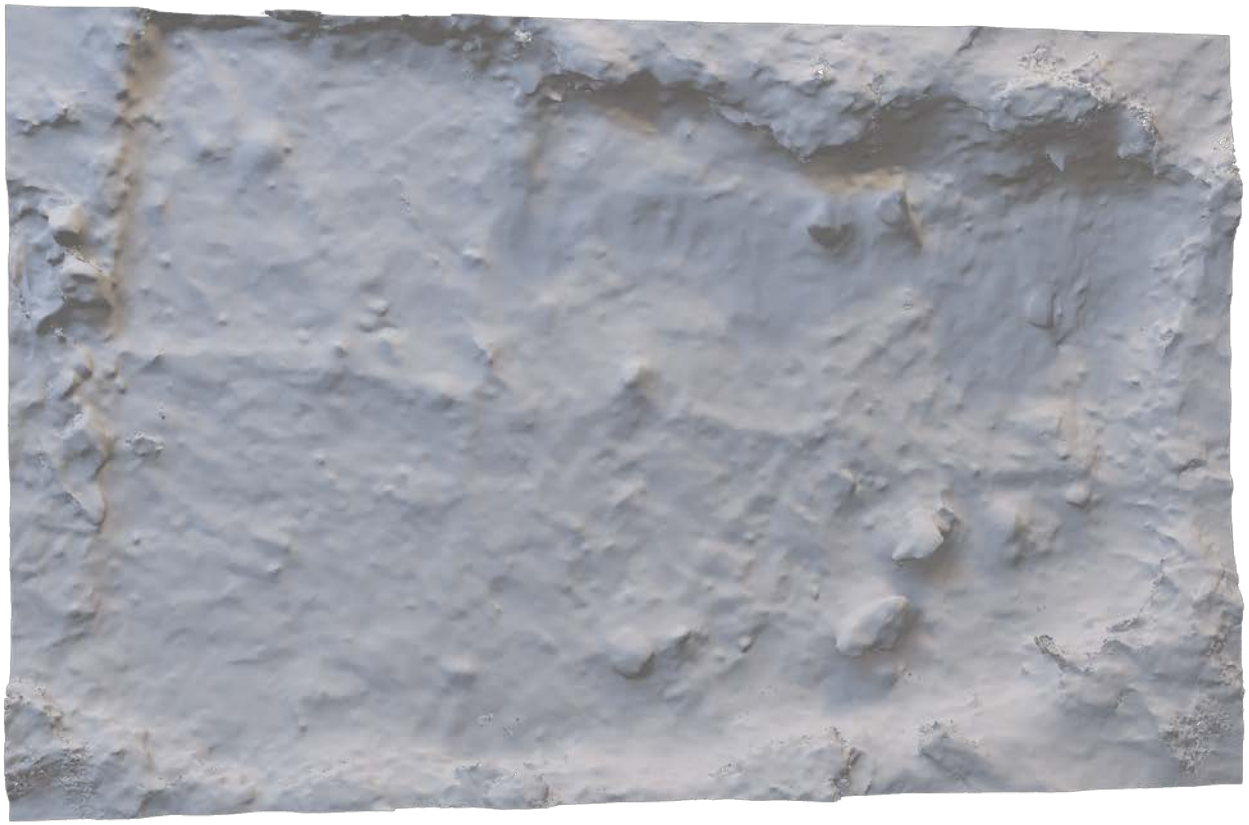

APPENDIX H: Level 1 Model Created by Consistent Graduate Student

APPENDIX I: Level 1 Model created by Author

APPENDIX J: Level 2 Model created by Random Graduate Student

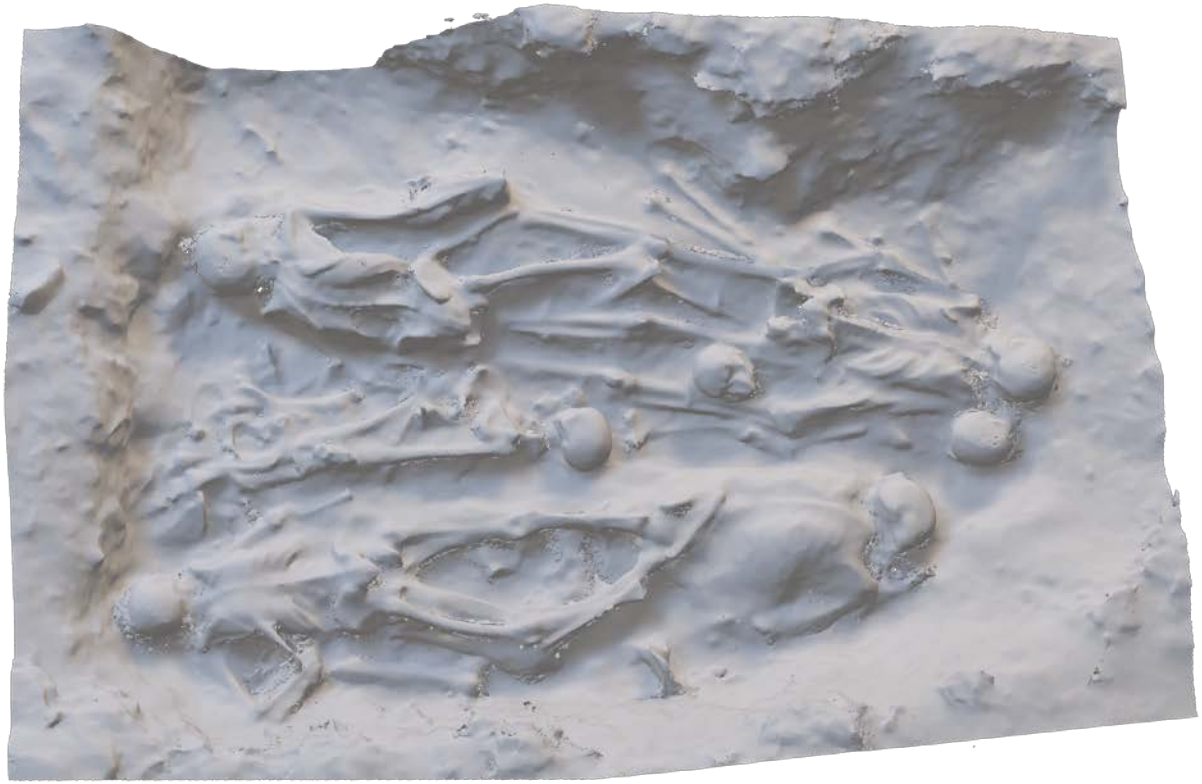

APPENDIX K: Level 2 Model created by Consistent Graduate Student

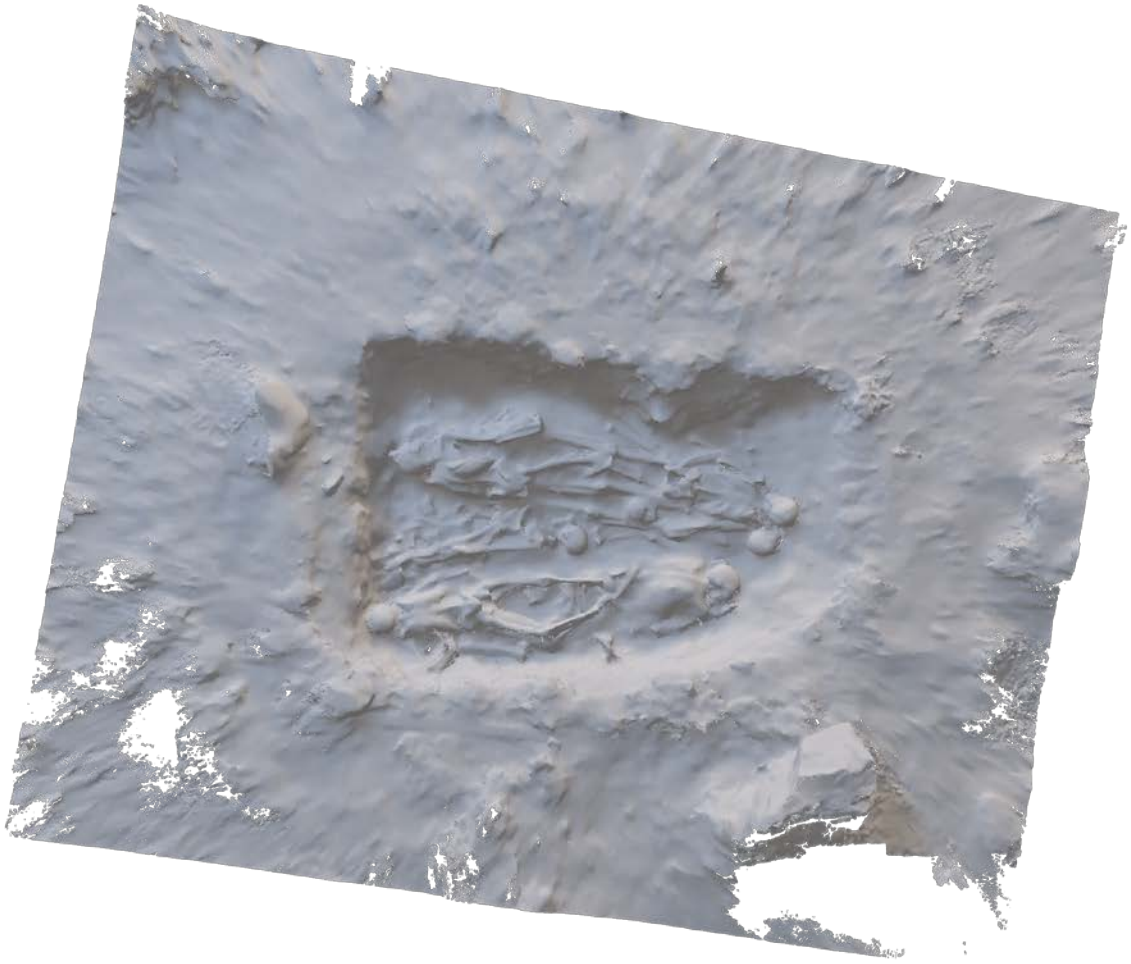

APPENDIX L: Level 2 Model created by Author

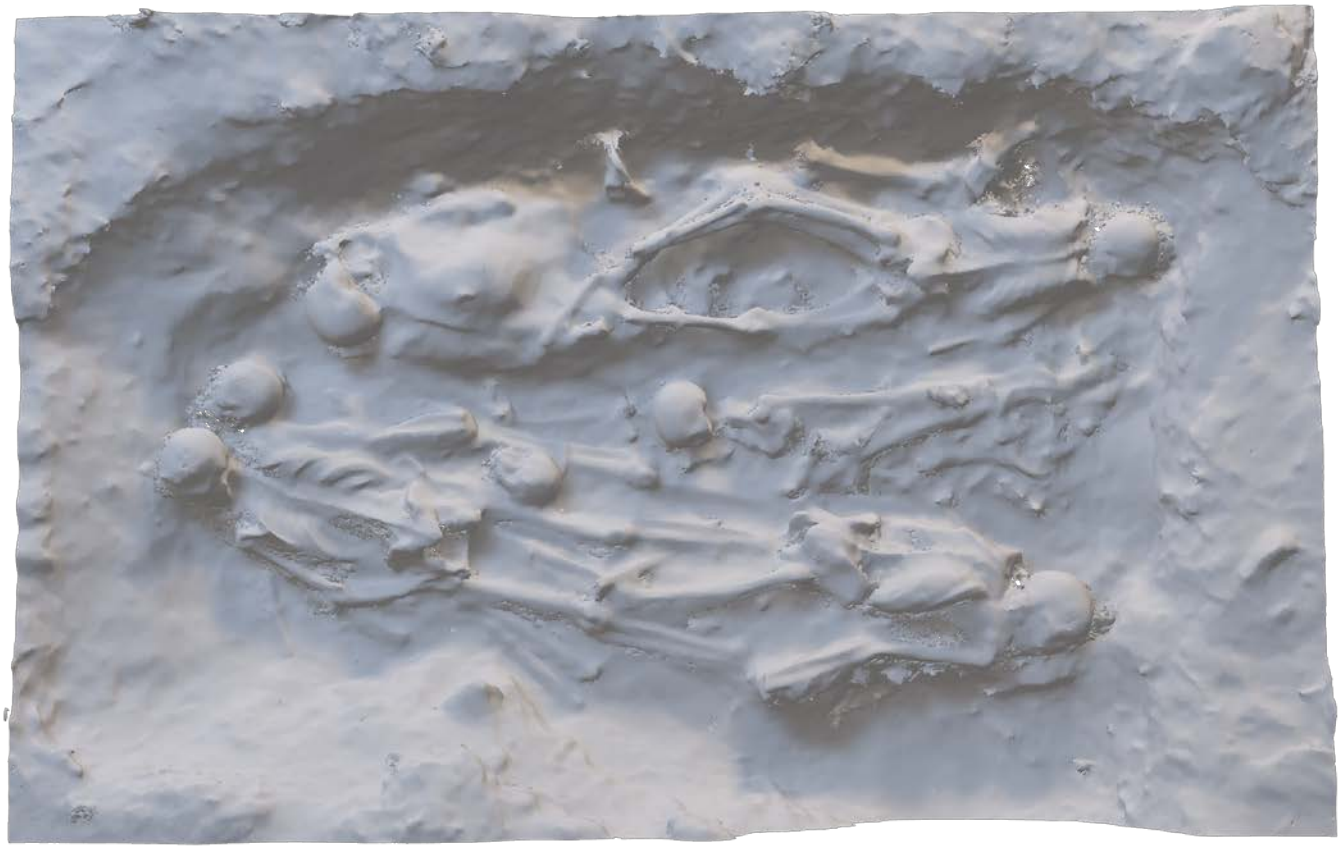

LITERATURE CITED

Agisoft PhotoScan Professional (1.3.2) (Software). (2017). Retrieved from http://www.agisoft.com/downloads/installer/.

Baier W, Rando C. 2016. Developing the use of Structure-from-Motion in mass grave documentation. Forensic Science International 261:19–25.

Bitelli G, Girelli VA, Marziali M, Zanutta A. Use of historical images for the documentation and the metrical study of Cultural Heritage by means of digital photogrammetric techniques. :6.

Bodnar BJ, DeAngelis QC. 1966. Paper-print Plotters. In: Manual of Photogrammetry. Vol. II. 3rd ed. ASPRS.

Boochs F, Heinz G, Huxhagen U, Müller H. LOW-COST IMAGE BASED SYSTEM FOR NON-TECHNICAL EXPERTS IN CULTURAL HERITAGE DOCUMENTATION AND ANALYSIS. :6.

De Reu J, De Smedt P, Herremans D, Van Meirvenn M, Laloo P, De Clercq W. 2014. On introducing an image-based 3D reconstruction method in archaeological excavation practice. Journal of Archaeological Science 41:251–262.

De Reu J, et al. 2013. Towards a three-dimensional cost-effective registration of the archaeological heritage. Journal of Archaeological Science 41:251–262.

Doneus M. 1996. Photogrammetrical applications to aerial archaeology at the institute for prehistory of the University of Vienna, Austria. In: Vol. XXXI. Vienna, Austria: International Archives of Photogrammetry and Remote Sensing. p 124–129. Available from: http://www.isprs.org/proceedings/XXXI/congress/part5/124_XXXI-part5.pdf

Douglass M, Lin S, Chodoronek M. 2015. The application of 3D photogrammetry for in-field documentation of archaeological features. Advances in Archaeological Practice 3:135–152.

Drap P, Seinturier J, Scaradozzi D, Gambogi P, Long L, Gauch F. 2006. Photogrammetry for virtual exploration of underwater archaeological sites. :6.

Evin A, Souter T, Hulme-Beaman A, Ameen C, Allen R, Viacava P, Larson G, Cucchi T, Dobney K. 2016. The use of close-range photogrammetry in zooarchaeology: Creating accurate 3D models of wolf crania to study dog domestication. Journal of Archaeological Science: Reports 9:87–93.

Falkner E. 1995. Aerial mapping: Methods and applications. CRC Press.

Galeazzi F. 2016. Towards the definition of best 3D practices in archaeology: Assessing 3D documentation techniques for intra-site data recording. Journal of Cultural Heritage 17:159–169.

Garstki K, Arnold B, Murray ML. 2015. Reconstituting community: 3D visualization and early Iron Age social organization in the Heuneburg mortuary landscape. Journal of Archaeological Science 54:23–30.

Georgiadis C, TSIOUKAS V, SECHIDIS L, STYLIANIDIS E, PATIAS P. Fast and accurate documentation of archaeological sites using in the field photogrammetric techniques. International Archives of Photogrammetry and Remote Sensing XXXIII:5.

Gonzalez MAM, Yravedra J, Gonzalez-Aguilera D, Palomeque-Gonzalez JF, Dominguez-Rodrigo M. 2015. Microphotogrammetric characterization of cut marks on bones. Journal of Archaeological Science 62:128–142.

Granshaw SI. 2016. Photogrammetric terminology: Third edition. The Photogrammetric Record 31:210–251.

Grussenmeyer P, Perdrizet F. 1996. Archeological photogrammetry with small format cameras: The survey of the forum vetus in Sarmizegetusa (Romania). International Archives of Photogrammetry and Remote Sensing XXXI:200–204.

Haglund WD. 2001. Recent Mass Graves, An Introduction. In: Advances in Forensic Taphonomy: Method, Theory, and Archaeological Perspectives. CRC Press. p 243–261.

Hartley R, Zisserman A. 2003. Multiple view geometry in computer vision. 2nd ed. Cambridge, UK ; New York: Cambridge University Press.

Hendrickx M, Gheyle W, Bonne J, Bourgeois J, De Wulf A, Goossens R. 2011. The use of stereoscopic images taken from a microdrone for the documentation of heritage - An example from the Tuekta burial mounds in the Russian Altay. Journal of Archaeological Science 38:2968–2978.

Howells W. 1973. Cranial variation in man.

Howland MD, Kuester F, Levy TE. 2014. Photogrammetry in the field: Documentin, recording and presenting archaeology. Mediterranean Archaeology and Archaeometry 14:101–108.

Jaklic A, Eric M, Mihajlovic I, Stopinsek Z, Solina F. 2015. Volumetric models from 3D point clouds: The case study of sarcophagi cargo from a 2nd/3rd century AD Roman shipwreck near Sutivan on island Brac, Croatia. Journal of Archaeological Science 62:143–152.

Kalantari M, Kasser M. 2003. Implementation of a low-cost photogrammetric methodology for 3D modelling of ceramic fragments. 2nd ed. Cambridge, UK ; New York: Cambridge University Press.

Katsianis M, Tsipidis S, Kotsakis K, Kousoulakou A. 2008. A 3D digital workflow for archaeological intra-site research using GIS. Journal of Archaeological Science 35:655–667.

Koenig CW, Willis MD, Black SL. 2017. Beyond the square hole: Application of Structure from Motion photogrammetry to archaeological excavation. Journal of Archaeological Science:1–27.

Koistinen K. 2000. 3D documentation for archaeology during Finnish Jabal Haroun project. In: Vol. XXXIII. Amsterdam, Netherlands: International Archives of Photogrammetry and Remote Sensing. p 440–445. Available from: http://www.isprs.org/proceedings/XXXIII/congress/part5/440_XXXIII-part5.pdf

Koutsoudis A, Vidmar B, Arnaautoglou F. 2013. Performance evaluation of a multi-image 3D reconstruction software on a low-feature artefact. Journal of Archaeological Science 40:4450–4456.

Martinez S, Ortiz J, Gil M. 2015. Geometric documentation of historical pavements using automated digital photogrammetry and high-density reconstruction algorithms. Journal of Archaeological Science 53:1–11.

Matthews N. 2008. Aerial and Close-Range Photogrammetric Technology: Providing Resource Documentation, Interpretation, and Preservation.

McCarthy J. 2014. Multi-image photogrammetry as a practical tool for cultural heritage survey and community engagement. Journal of Archaeological Science 43:175–185.

Patias P, Sylaiou S, Sechidis L, Spartalis I, Grussenmeyer P, Meyer E, Landes T, Alby E. A proposed low-cost system for 3D archaeological documentation. :6.

Porter ST, Roussel M, Soressi M. 2016. A simple photogrammetry rig for the reliable creation of 3D artifact models in the field. Advances in Archaeological Practice 4:71–86.

RStudio Team, 2015. RStudio: Integrated Development for R. RStudio, Inc., Boston, MA URL http://www.rstudio.com/.

Rua H, Alvito P. 2011. Living the past: 3D models, virtual reality and game engines as tools for supporting archaeology and the reconstruction of cultural heritage - the case-study of the Roman villa of Casal de Freiria. Journal of Archaeological Science 38:3296–3308.

Sanger M. 2015. Determining depositional events within shell deposits using computer vision and photogrammetry. Journal of Archaeological Science 53.

Schmitt S. 2001. Mass graves and the collection of forensic evidence: Genocide, war crimes, and crimes against humanity. In: Advances in Forensic Taphonomy: Method, Theory, and Archaeological Perspectives. CRC Press. p 277–292.

Simmons T. 2001. Taphonomy of a Karstic Cave Execution Site at Hrgar, Bosnia-Herzegovina. In: Advances in Forensic Taphonomy: Method, Theory, and Archaeological Perspectives. CRC Press. p 263–275.

Stal C, Van Liefferinge K, De Reu J, Docter R, Dierkens G, De Maeyer P, Mortier S, Nuttens T, Pieters T, van den Eijnde F, van de Put W, De Wulf A. 2014. Integrating geomatics in archaeological research at the site of Thorikos (Greece). Journal of Archaeological Science 45:112–125.

Thompson MM. 1966. Introduction to Photogrammetry. In: Manual of Photogrammetry. Vol. I. 3rd ed. ASPRS.

Tuller H. 2012. Mass graves and human rights: Latest developments, methods, and lessons learned. In: A Companion to Forensic Anthropology. Wiley-Blackwell. p 157–175.

Tuller H, Duric M. 2006. Keeping the pieces together: Comparison of mass grave excavation methodology. Forensic Science International 156:192–200.

Tuller H, Hofmeister U. 2014. Spatial analysis of mass grave mapping data to assist in the reassociation of disarticulated and commingled human remains. In: Recovery, Analysis, and Identification of Commingled Human Remains. Humana Press. p 7–32.

Verhoeven G. 2011. Taking Computer Vision Aloft - Archaeological Three-dimensional reconstruction from aerial photographs with Photoscan. Archaeological Prospection 18:67–73.

Verhoeven G, Doneus M, Briese C, Vermeulen F. 2012. Mapping by matching: a computer visio-based approach to fast and accurate georeferencing of archaeological aerial photographs. Journal of Archaeological Science 39:2060–2070.

Walker S, Alspaugh D. 2013. A brief history of photogrammetry. In: Manual of Photogrammetry. 6th ed. Bethesda, Maryland: American Society for Photogrammetry and Remote Sensing. p 1–62.

Zobeck TS. 1983. Postcraniometric variation among the Arikara.